Probabilistic Adaptive Power Pinch Analysis for Islanded Hybrid Energy Storage Systems

Nyong-Bassey Bassey Etim[a,1], Damian Giaouris[b]

[a] *Department of Electrical and Electronics Engineering, College of Engineering and Technology, Federal University of Petroleum Resources, Nigeria*
[b] *School of Engineering, Newcastle University, Newcastle NE1 7RU, United Kingdom*

ABSTRACT

Hybrid energy storage systems involve the integration of multifarious energy storage technologies which have complementary operational characteristics. Although the incorporation of hybrid energy storage systems can suppress renewable energy intermittency and improve energy supply; control and coordination become more challenging. By integrating more assets and more functions in the system, the complexity becomes prohibiting and hence new versatile and scalable methods must be employed. The authors have in the past proposed a graphical energy management strategy based on the power pinch analysis framework to address this challenge but was contingent on average energy demand and supply profile that reflects only a single scenario case study. This paper proposes a probabilistic adaptive power pinch analysis paradigm for energy management of isolated hybrid energy storage systems with uncertainty, which is implemented in a model predictive receding horizon. The proposed method uses multistate stochastic power grand composite curves realised from the integration of distinct energy demand and supply profiles randomly sampled from historic data via Monte Carlo simulation. Thus, in a predictive horizon, the multiple possibilities which the state of the energy storage can attain must jointly satisfy a probabilistic chance constraint factor with necessary decisions inferred in the control horizon to negate uncertainty. The proposed probabilistic method was further improved by a correction mechanism that minimises the mean squared error between the actual and predicted state of charge of the battery. The performance of probabilistic power pinch analysis was tested on a hybrid energy storage system with renewable energy sources, a battery, a fuel cell and an electrolyser. The results clearly demonstrate improved robustness to Gaussian uncertainty than a day ahead power pinch analysis reference as over-dis/charging the battery and carbon emission was reduced by 98%, 22% and 100% respectively but, necessitates allocating more hydrogen resources.

Keywords: Hybrid Energy Storage Systems; Energy Management Strategies; Model Predictive Control; Monte Carlo simulation; Power Pinch Analysis.

---

[1] Corresponding Author at *Department of Electrical and Electronics Engineering, College of Engineering and Technology, Federal University of Petroleum Resources, Nigeria.*
E-mail address: NyongBassey.Bassey@fupre.edu.ng

The short version of this paper was presented at PEMD 2018, Liverpool, United Kingdom. This paper is a substantial extension of the PEMD2018 Conference paper.

Nomenclature

$AEEND$	Available excess energy for the next day
BAT	Battery
C_l	The capacity of accumulator l
DSL	Diesel generator
EL	Electrolyser
FC	Fuel cell
HT	Hydrogen Tank
LD	Load
MAE	Minimum absorbed energy
$MOES$	Minimum outsourced energy supply
$SOAcc_l^n$	State of accumulator l
S_{Lo}^l	Lower pinch limit or utility
S_{Up}^l	Upper pinch limit or utility
POW	Power flow
$PGCC$	Power grand composite curve
$\mathcal{N}$	Zero mean Gaussian uncertainty
$\mathcal{U}$	Input $\in R^{mx1}$
WT	Water tank
Δk	*Time interval*
$\eta_{CV},\eta_{PV},\eta_{FC},\eta_{EL}$	DC converter, PV panel, fuel cell, electrolyser efficiency factors
$\varepsilon_i\,(k)$	Binary variable for the state of the ith dispatchable unit
$\rho_i^{i_c}$	The binary variable related to the temporal conditions of the accumulator

Subscripts/superscripts

$SOAcc$	Accumulator or energy storage
k	Time step
i	Index of Converter
l	Accumulator
max	maximum
min	minimum
$m\,,n$	Model and the plant respectively
i_c	A set of controllable energy converter elements for PoPA targeting

1. Introduction

The deployment of renewable energy systems (RES) such as photovoltaic (PV) systems have grown considerably popular as a global inclination for decreasing greenhouse gas emissions [1]. Nevertheless, while RES delivers decent to large-scale energy output, particularly in off-grid locations [1, 2], the RES energy output is only available intermittently [3, 4] and cannot provide a 24-hour load demand requirement due to weather variations [1]. Thus RES used exclusively is unreliable, necessitating the incorporation of energy storage (ES) to offset energy variations or uncertainty, improve power quality, especially in islanded systems [5].

To simultaneously improve RES reliability and mitigate load demand uncertainty, multiple ES technologies (e.g. battery (BAT) and hydrogen (H2)) with complementary properties (such as life cycle, seasonality, power, energy density, etc.) are frequently combined to realize the concept of hybrid energy storage systems (HESS) [6, 7]. Some common HESS configurations with RES for off-grid applications are super-capacitor (SC)/ battery (BAT) [8, 9], fuel cell (FC)/BAT [10, 11], FC/SC [12] and BAT/FC/SC [13, 14].

Particularly an experimental RES-BAT-Hydrogen-based islanded HESS conceptualized and built collaboratively by SUNLIGHT and CERTH in Xianti, Greece [7, 15] is used as a case study in this research work. The experimental HESS comprises; RES such as photovoltaic panels (PV), non-RES such as a DSL for backup supply, electrical load demand (LD), fuel cell (FC), electrolyser (EL), and battery storage (BAT) and a compressor between the EL and HT which has been omitted due to low voltage application. The principal operation of the islanded HESS is complimentary and regenerative, such that excess energy from the PV is stored in the BAT until fully charged, and while the BAT is fully charged (i.e. the state of Charge of the battery $SoAcc_{BAT}$ >90%). Further, excess energy from the PV is transformed to hydrogen by the EL for storage and vice-versa to charge the BAT (i.e. $SoAcc_{BAT} < 30\%$) by the FC during such periods of energy deficit. The backup DSL is activated only when the BAT state of charge is below 20% and deactivated once the BAT is charged above 30%. Figure 1, shows the schematic diagram of the experimental HESS.

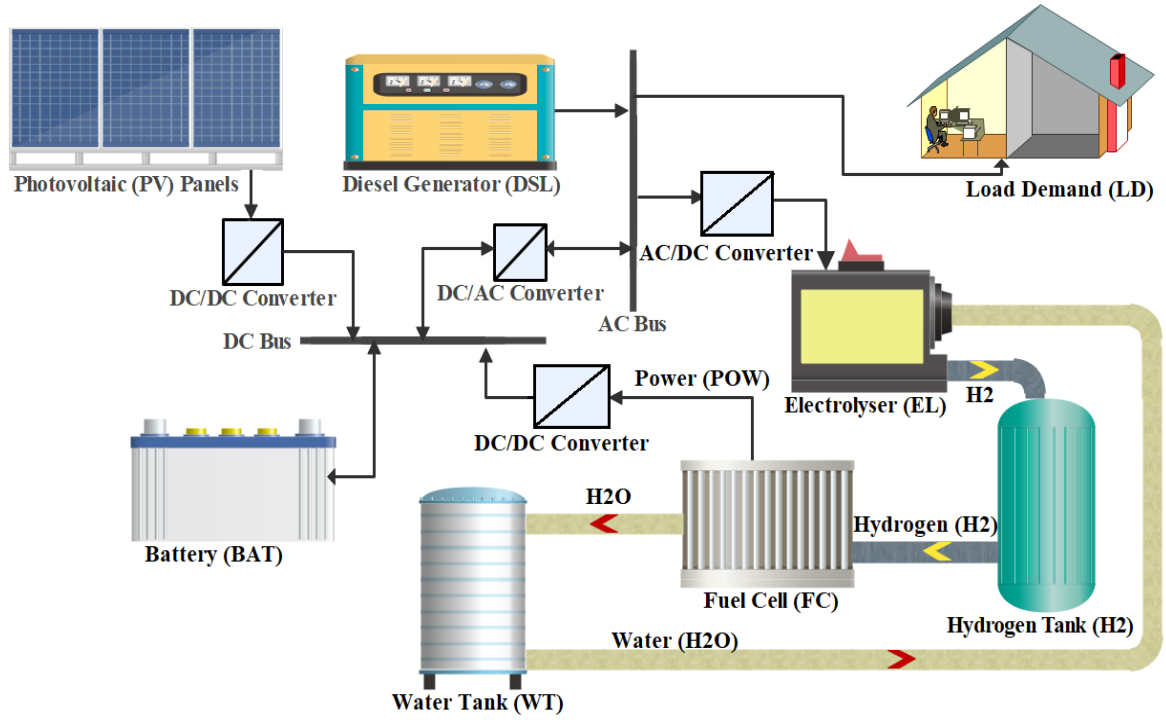

Fig. 1: Schematic diagram of the experimental HESS used as a case study [7].

Despite the benefit of enhanced energy reliability HESS can offer, it imposes challenges with regards to controlling and coordinating the transformative flow of varied energy/material [16], coupled with the problem of RES variability and load demand uncertainty, necessitates the use of an energy management strategy (EMS) [17].

1.1 Conventional Energy Management Strategies for HESS

EMS algorithms orchestrate the behaviour of the energy system to improve one or more performance objectives, such as operational cost, RES penetration, own-consumption, self-sufficiency etc. while satisfying technical operational constraints [18]. Majority of these EMS algorithms are based on if-else-then logic propositions [19], fuzzy logic control (FLC) [20], dynamic programming (DP) [21], stochastic optimisation (SO) [22], robust optimization (RO) [23, 24], evolutionary algorithms (EA) [25], neural network (NN) [26], reinforcement learning (RL) [27] and advanced model predictive control (MPC) [28].

Specifically, heuristic logical rule-based EMS was used to reduce CO2 emissions, minimise total operating cost and maximise RES penetration in BA-RES [19]. Nevertheless, while the rule-based EMS are computationally efficient for online control of energy systems operation, calibration is a challenge due to uncertainty in a plethora of operational pre-conditions [29]. Further, EMS based on FLC optimally coordinated energy flow in a BAT-SC HESS [30] and a BAT-ultra-capacitor HESS [31]. While the FLC offers robustness, crafting the logical rules requires experience. In [23] a stage-by-stage

robust optimisation EMS was proposed to minimise the total operational cost ensuring a combined cooling, heating, and power MG while negating uncertainty under the worst-case scenario.

In [22] DP EMS was proposed to mitigate DC-link voltage variation due to intermittent RES and stochastic load in a HESS comprising a battery bank and ultra-capacitor grid-connected HESS microgrid. In [24] a dual-stage robust MPC optimisation is proposed, to reduce the impact of load demand and RES uncertainty in an islanded MG. However, the robust optimisation method is considered a pessimistic approach and can result in over-budgeting in real-world applications [32]. In [33] a three-layered hierarchical EMS for HESS with different temporal resolutions (Day-ahead (DA), quarterly and minute scale) based on mixed-integer non-linear programming, SO-MPC, and Pontrygin's minimum were to meet operational cost, energy balance and reduce power fluctuations respectively in a HESS. More so, stochastic and chance-constrained based optimisation has been applied in [34, 35]. In [36] real-time RL based EMSs were used to enhance the lifecycle of BAT-SC HESS in an electric vehicle and in [37] to optimally control the charge and discharge cycle and also suppress disturbances ensuing from HESS integration in the microgrid.

On the one hand, DP and optimisation based EMSs can achieve global optimality, however, they are computationally cumbersome and intractable and offer only a final solution [27], hence unsuitable as an online EMS [29]. On the other hand, EMS based on neural network alone are too simple to offer realistic gains in controlling HESS [29], RL-EMS used alone may suffer from sub-optimality [27] and the performance of MPC based EMS [28] largely depends on prediction accuracy [29].

Further, to address these limitations, recently a graphical power pinch (PoPA) EMS [8, 27, 38, 39] emerged. The PoPA is inspired by the classical pinch analysis (PA) a process integration technique that was first introduced by Linnhoff and Flower [40] for heat integration and energy recovery in heat exchanger networks [41]. The power grand composite curve is a simple graphical PoPA tool realised via the integration of energy demand and supply with time to precisely identify and conservatively match energy deficit and excess energy recovery targets called pinch points with minimum resources. This aids the construction of an EMS that enables internal energy recovery rather than use non-RES. The PGCC has mostly been utilized to identify energy requirements in deterministic scenarios to improve HESS performance [27].

1.2 Power Pinch analysis for Energy Systems sizing and planning

Pinch analysis (PA) extends beyond the synthesis of designing and retrofitting HEN [42] to the expansion of cleaner cost-effective optimal resource conservation networks [43] such as water recycling [44], mass [45], gas [46], hydrogen [47] and quite recently sizing [48], design and planning [49] of power systems. In [50] energy demand and supply were integrated to form the PoPA grand composite curve tool which aided the optimal sizing of an islanded power generating system. In [51] chance constraint programming with PoPA concept validated via MCS was used to size PV in a RES-BAT MG

considering uncertainty. In [48] composite curves were used to determine the rated power required to satisfy demand in hybrid power systems while minimizing electricity cost.

1.3 Power Pinch analysis for EMS in HESS

Despite the fact that PoPA has been used for sizing, planning and design of energy systems, recently it was used for energy management of HESS islanded MG. The first PoPA EMS [8], was realised by shaping a graphical power grand composite curve (PGCC) and further applied in [38] within a day ahead (DA) model predictive control (MPC) framework. The DA-PoPA EMS conservatively targeted deficit and excess energy recovery targets by shaping the PGCC in a predictive horizon and consequently effecting the optimal decisions in a control horizon on an islanded HESS MG. Therefore, the advantages of the DA-PoPA method were clearly demonstrated in [38]. Nevertheless, a limitation of the DA-PoPA in [38] was the assumption of perfect weather and load demand forecast without consideration for uncertainty, which is now being enhanced in this research work. Further, this limitation was identified and addressed via an adaptive PoPA EMS [39] which performed deficit energy targeting and excess energy recovery in a receding horizon MPC and further enhanced by an intelligent agent approach, the 'RL+adaptive PoPA' in [27]. The RL adaptive PoPA treated the issue of uncertainty in HESS as a Markov decision process (MDP), where an intelligent agent acts optimally to infer EMS which maximises a given reward in a state by avoiding over-dis/charging of the BAT. Nonetheless, the RL agent's prior knowledge of the MDP was contingent on the agent training on the deterministic adaptive model.

1.4 Motivation for a probabilistic PoPA EMS

The above EMS algorithms have largely been limited to deterministic scenarios (such as average energy demand and supply profiles) that may not reflect real-world complexity and lead to inconsistent results. Nevertheless, Monte Carlo simulation (MCS) can account for uncertainty via probabilistic risk assessment of reliability [18] and also improves conservatism [52].

Several studies have suggested strategies for robustness to uncertainty in power systems energy reserve planning [53] and peak load shaving [54], economic risk analysis in [55], and RES sizing [51]. Specifically, in [51] the minimum area of a solar panel required to conservatively satisfy load demand within a specified reliability threshold was determined based on PoPA and chance constraint programming respectively, and then validated via MCS.

It is clear that weather intermittency and stochastic consumer's load pattern, pose risk to the reliability of energy supply and demand balance. Nevertheless, an active probabilistic EMS should suffice for a better realistic assessment of uncertainty in HESS.

1.3. Main Contributions and Novelties

From the aforementioned, it is also clear that PoPA EMS for HESS, have mostly been via a deterministic approach which can be limiting and insufficient in dealing with uncertainty especially when the available historical data demonstrates stochastic variations.

This paper proposes an improved PoPA EMS framework for hybrid energy storage systems, particularly under Gaussian uncertainty. More so, historical data of load demand and PV variation are exploited to enhance robustness to uncertainty using a systems-level EMS based on a probabilistic adaptive PoPA by conservatively dis/charging the BAT and preserving its life cycle with intermittent RES and limited hydrogen resources while satisfying stochastic load demand in an islanded/off-grid HESS.

Specifically, the main contributions in this paper are as follows:

I. A probabilistic adaptive PoPA approach via Monte Carlo simulation with chance constraint within a receding horizon MPC framework for EMS of islanded HESS is proposed. In a prediction horizon, MCS runs n-multi-state stochastic graphical PGCCs of the BAT. Thereafter, the safety and desired operating limits ($30\% \leq SOAcc_{BAT}^{n} \leq 90\%$) of the PGCCs of the BAT which should never be violated are assessed over a reliability chance constraint. Consequently, hydrogen assets; FC and EL are conservatively and optimally dispatched in advance in the control horizon to negate the effects of uncertainty.

II. An elegantly formulated recursive least square probabilistic adaptive PoPA MPC algorithm using estimation error correction factor to mitigate uncertainty by minimising the error between actual and estimated energy storage's state of charge $SOAcc_{BAT}^{m}$ is also presented. This basically, establishes an equilibrium between the actual and estimated $SOAcc_{BAT}^{m}$ such that the estimated $SOAcc_{BAT}^{m}$ is corrected. Furthermore, two recursive least square probabilistic (RLS-P) PoPA models, ($y = Ax$ and $y = Ax + B$) were investigated to establish the effect of increasing terms in the (RLS-P) adaptive PoPA model to counteracting the forecast uncertainty.

III. The proposed probabilistic adaptive PoPA algorithms have been compared to a deterministic DA-PoPA [38] reference model and other existing adaptive PoPA EMS [27]. The probabilistic (RLS-P) PoPA with a multiplicative mechanism, negated Gaussian uncertainty the most and compared to a reference DA-PoPA EMS over-dis/charging the battery and carbon emission were reduced by 98%, 22% and 100% respectively.

IV. A battery degradation model which accounts for the total degraded life cycles under PoPA EMSs was synthesised based on the cumulative sum of the normalised reciprocal of the total battery life

cycle model [72] derived with respect to the battery's depth of discharge (DoD) and multiplied by the range of equivalent DoD cycles that were counted using a rainflow-counting algorithm [71].

The rest of the paper is structured as follows: Section 2 briefly describes the Power Pinch analysis concept and the Monte Carlo simulation. Section 3 presents the formalisation of the receding Probabilistic adaptive MPC-PoPA concept and includes the recursive least square estimation approach for correcting the estimated energy storage's state of charge $SOAcc_{BAT}^{m}$. The results and discussion are presented in Section 4, and Section 5 offers a conclusion.

2. Methodology

2.1 Power Pinch Analysis for Energy Management of HESS

The principles of adaptive power pinch analysis for energy management which is well illustrated in [27, 38], basically involves the use of a power grand composite curve (PGCC) tool which is the net result of both energy demand and supply. The PGCC is analogous to the grand composite curve (GCC) in heat exchanger networks (HEN) which is an integration of heat transfer between hot (sources) and cold (demand) streams as a function of temperature (quality) [50].

The predicted PGCC expressed as a plot as illustrated in Figure 2(a) (black dotted line) infers energy deficits and excess expressed for specific operating limits in the HESS. Since the lowest point of the PGCC $SMin$ is below (or violates) the first lower limit SLo (i.e. $SLo = 30\%$) a time $k + 2$, this indicates energy deficit in a specific HESS energy storage such as the BAT (i.e. $SOAcc_{BAT} < SLo$). Consequently, the FC is activated to charge the battery while, the DSL is activated if $SMin$ is below a second limit ($SMin < 20\%$) to protect the battery's life time. Similarly, since the PGCC is above (or violates) the upper operating limit SUp (i.e. $SUp = 90\%$) at time $k + 11$, this indicates the excess which must be recovered and transformed for storage (such as electrical energy to hydrogen, H2) for future use. Specifically, the energy deficit in the HESS can occur in the early hours of the day as a result of the BAT state of Charge ($SOAcc_{BAT}$) being below 30% and the PV not having sufficient exposure to solar irradiation. Thus, by shaping the predicted PGCC to pinch on SLo, the energy deficit at time $k + 2$ is averted by charging the BAT in advance at time k with the necessary minimum outsourced energy supply (MOES). The MOES is supplied typically with the FC, indicated by the upward 'green' arrow shifting the blue dashed PGCC plot in Figure 2(b). Likewise, the excess energy from the PV when the BAT is sufficiently charged (i.e. $SOAcc_{BAT} > 90\%$), termed minimum absorbed energy (MAE) is identified in advance at time $k + 11$ (or at least an hour before the violation of SUp) and transformed to hydrogen for storage by an EL (indicated by the downward 'red' arrow shifting the yellow dashed shaped PGCC plot in Figure 2(c)) for use at a later period of energy deficit. Furthermore, the life cycle of the PGCC is preserved by equalising the available electricity energy for the next day (AEEND) to

the state of charge at the first hour at time $N-1$ as indicated by the purple plot shown in Figure 2(d). Thus, the energy deficit and excess, as well as the AEEND are identified in a predictive receding horizon with hourly interval Δk which spans 24h $\in [k:N]$ where k is the i^{th} hour in a day and N denotes the end of the day (or 24th h). While, in a control horizon, the suitable EMS obtained in the predictive horizon is deployed in advance with a DA-PoPA and if there is forecast error +/-5%, the PGCC is recomputed using the adaptive PoPA in the receding horizon to negate the uncertainty as shown in Figure 2(e) and 2(f) respectively.

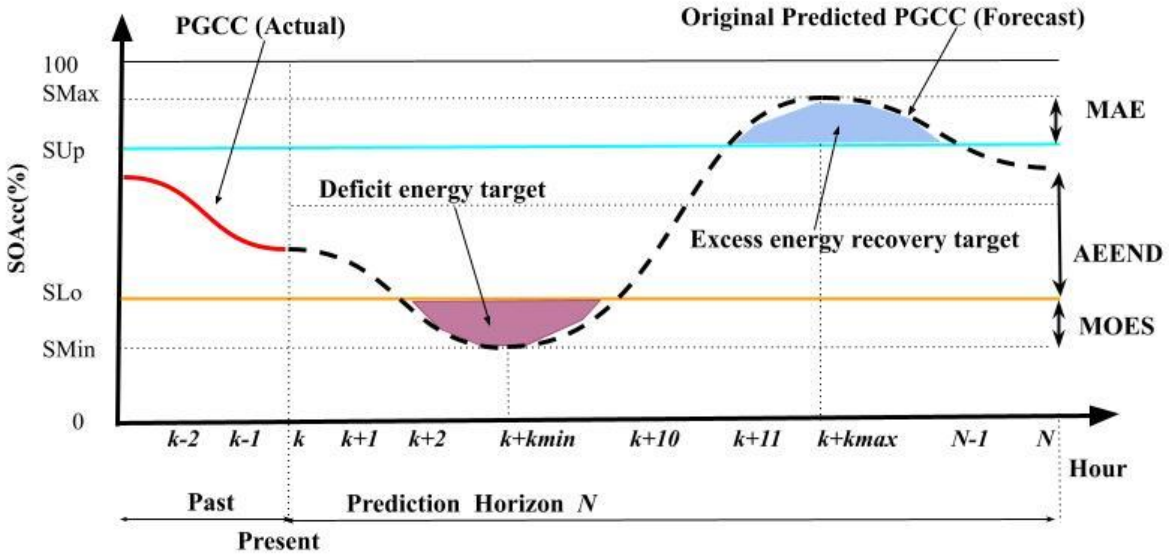

Fig. 2(a): PGCC realised in the prediction horizon

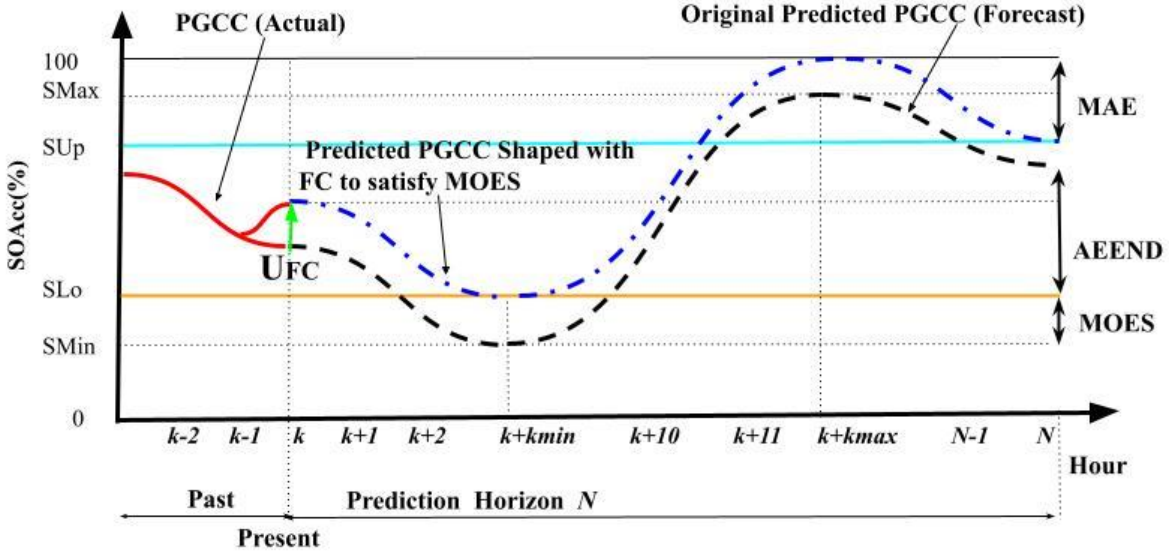

Fig. 2(b): illustration of PGCC concept for deficit energy targeting with FC to match MOES

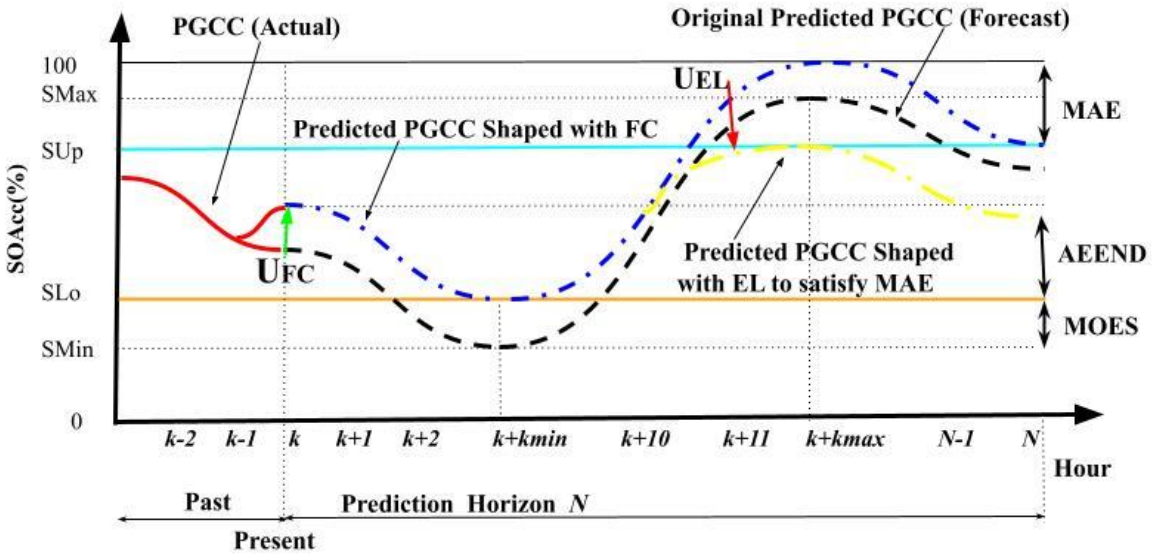

Fig. 2(c): illustration of PGCC concept for excess energy recovery with EL to match MAE

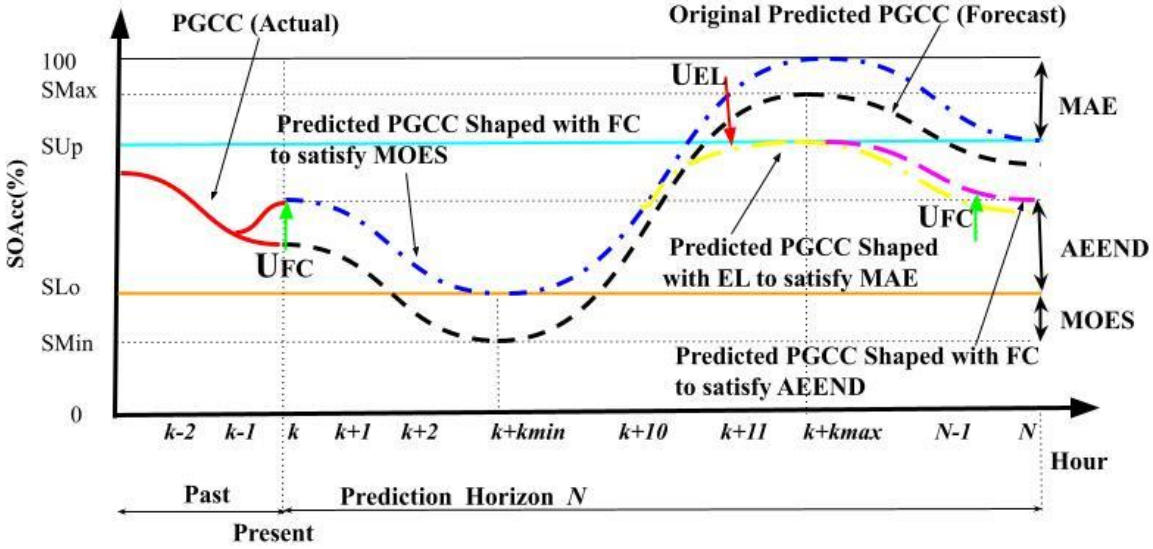

Fig. 2(d): AEEND illustration for lifecycle preservation

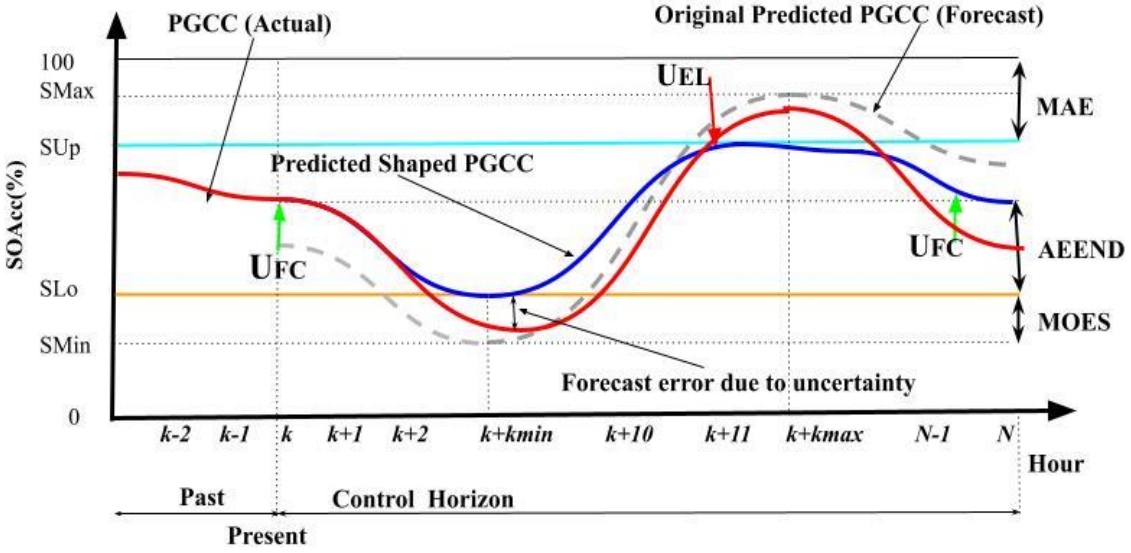

Fig. 2(e): Effect of uncertainty with DA-PoPA PGCC shaped in control horizon

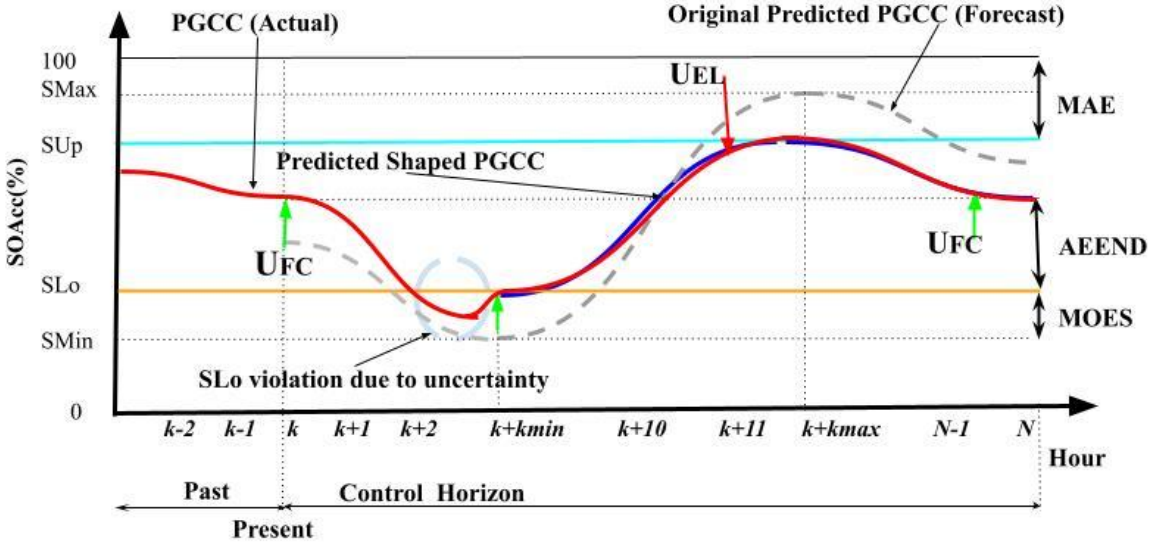

Fig. 2(f): PGCC shaped with Adaptive-PoPA in control horizon

2.1 Monte Carlo Simulation

The PoPA EMS, ensures a balance between energy demand and supply, as excess supply and undersupply of energy result in wastage and degradation of the storage assets, respectively. Unfortunately, due to the uncertainty associated with RES and load demand, which is often probabilistic and may exhibit daily, seasonal, and geographical variability, forecast error may be introduced [56]. Thus, satisfying the energy systems constraints can become challenging to achieve using a deterministic model. Furthermore, deterministic models are often considered with a set of deterministic input

variables and upon the occurrence of each variation, it becomes imperative to repeat the simulation process to obtain a new solution [57]. Therefore, if adequate historical and statistical evidence regarding the uncertain parameter is available, it can be leveraged using powerful computational tools such as the Monte Carlo Simulation.

Monte Carlo simulation uses repetitive sampling of random input parameters to statistically parameterise the uncertainty associated with a dependent variable via a probability distribution. The Monte Carlo integration is expressed mathematically in equation (1) as follows [58, 59];

$$I = \int f(x)dx \tag{1}$$

Where, I is the integral of a function with input random variable x.

Furthermore, a good approximate estimation of $I(f)$ can be obtained such that by repeating the simulation in consonance with the theory of large numbers, the expectation $E\{f(X)\}$ of the random variable $f(X)$ is as follows in equation (2);

$$E\{g(X)\} = \frac{1}{n}\sum_{j=1}^{n} g(x)f(x_j) \tag{2}$$

Where x is the value of a stochastic variable drawn from a normal distribution $f(x_j)$ such that $X \in \mathbb{R}$ are independent and identically uniformly distributed i.i.d and $g(x)$ is a function.

3. Probabilistic Adaptive Power Pinch Analysis

The adaptive PoPA [39] is recast in a probabilistic framework [56] in this section. Multistate stochastic PGCCs obtained by MCS are used to form probabilistic chance-constrained certainty bounds on the $SOAcc$ to proffer robustness to uncertainty. Furthermore, to enhance the EMS, an online recursive correction factor which is determined based on the least-squares error approach via the residual error between the actual and predicted $SOAcc_{BAT}^{m}$ is used to update the $SOAcc_{BAT}^{m}$. The chance constraint sizing approach presented in [51], is used to determine the minimum solar panel array area in the PoPA framework, primarily targeted reliability of the deterministic load demand being met as well as the battery being charged. However, the energy management aspects if the BAT becomes fully charged and the utilisation of the excess energy were not considered. Thus, inspired by [39, 51] an adaptation is presented by defining the adaptive energy management algorithm in a recursive least square probabilistic MCS chance-constrained framework. Furthermore, the consequence of excess energy in the system, represented by the overcharging of the BAT ($SOAcc_{BAT}^{n}$>90%) which can damage the BAT and energy deficit due to over-discharging the BAT ($SOAcc_{BAT}^{n}$<30%) which degrades BAT life cycle, as well as AEEND for preservation of the life cycle of the BAT are considered in the chance constraints evaluated with the MCS.

3.1 Probabilistic Adaptive Power Pinch Analysis Formulation

Firstly, the deterministic PGCC computed in the predictive horizon as described in section 2.1 is expressed in an adaptive receding horizon model predictive framework, with state error correction as follows in (3):

$$SOAcc_l^m(k) = \min_{U_c} \sum_{k=1}^{N} \left[SOAcc_l^m(k-1) + \left(\sum_{X_l \in E_{tr}} \mathcal{F}_{l \leftarrow X_l}^j(k) - \sum_{Y_l \in E_{tr}} \mathcal{F}_{l \rightarrow Y_l}^j(k) \right) * \frac{\Delta k}{C_l} \right] \quad (3)$$

Let the vector $mSOAcc_l^m$ contain elements of corresponding time series state of charge of the Battery as follows in (4):

$$mSOAcc_l^m := \langle SOAcc_l^m(k),\ SOAcc_l^m(k+1),\ SOAcc_l^m(k+2) \quad \dots \quad SOAcc_l^m(N) \rangle \quad (4)$$

Secondly, by decoupling the energy-consuming assets $Y_l \in \{LD, EL\}$ with emphasis on $l \in \{\text{BAT}\}$ and corresponding energy flow $\mathcal{F}_{l \rightarrow Y_l}^j$, the $SOAcc_{BAT}^m$ is defined as a function of the flow of energy from the Battery to an i.i.d random load $LD^i \in (LD^1, \dots, LD^M)$ in (5):

$$SOAcc_l^m(k) = \sum_{i=1}^{M} \sum_{k=1}^{N} \left[SOAcc_l(k-1) + \left(\sum_{X_l \in E_{tr}} \mathcal{F}_{l \leftarrow X_l}^j(k) - \left[\mathcal{F}_{l \rightarrow EL_l}^j(k) + (\mathcal{F}_{l \rightarrow LD_l}^j(k) * f_X\left(LD^i(k)\right) \right] \right) * \frac{\Delta k}{C_l} \right] \quad (5)$$

Where, $f_X\left(LD^i\right)$ is the probability density of the random variable LD, estimated using a non-parametric kernel density estimator, KDE in MATLAB and subscript indicates the i^{th} sample of the random variable drawn from the prior distribution.

Furthermore, a matrix that contains mn-multi-state elements of $SOAcc_l^m$, is defined as follows in (6):

$$MSOAcc_l^m = \begin{bmatrix} SOAcc_{1,1} & SOAcc_{1,2} & \cdots & SOAcc_{1,N} \\ SOAcc_{2,1} & SOAcc_{2,2} & \cdots & SOAcc_{2,N} \\ \vdots & \vdots & \ddots & \vdots \\ SOAcc_{M,1} & SOAcc_{M,2} & \cdots & SOAcc_{M.N} \end{bmatrix} = SOAcc(i,j) \in R^{M,N} \quad (6)$$

$* Subscript\ l\ in\ SOAcc_{mn}\ has\ been\ omitted\ in\ equation\ (6)\ for\ conciseness$ and $m, n \neq M, N$.

Therefore, the matrix comprises the posterior distribution of the multistate stochastic $SOAcc_l$ PGCCs as shown in Figure 3(a) for each consumer load, sampled randomly from the prior distribution.

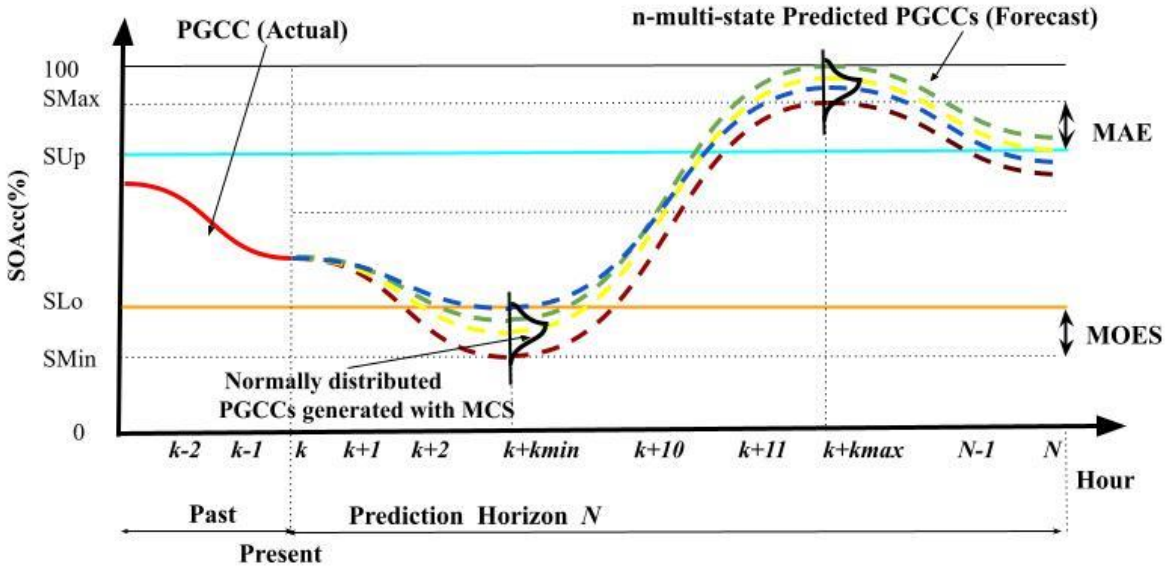

Fig. 3(a) : n-Multistate normally distributed PGCCs predicted with Monte Carlo Simulation.

Furthermore, the probabilistic PoPA performed with $z \in [1{:}L]$ iterations until the lower and upper limits expressed using the chance constraints are matched as follows (7):

$$SOAcc_l^m(i,j)^z = \sum_{z=1}^{L}\sum_{i=1}^{M}\sum_{k=1}^{N-1}\left[SOAcc_l(k-1) + \left(\sum_{X_l \in E_{tr}} \mathcal{F}_{l\leftarrow X_l}^{j(i)}(k) - \sum_{Y_l \in E_{tr}} \mathcal{F}_{l\rightarrow Y_l}^{j(i)}(k)\right) * \frac{\Delta k}{C_l}\right] \tag{7}$$

Thus, analytically by plotting the cumulative density function at each time step k, the probability, Pr of violating the lower limits (i.e. over-discharging the BAT beyond its normal depth of discharge to protect the battery's life cycle from deteriorating and prevent usage of non-RES or backup DSL) is constrained by the chance factor α_1 in (8):

$$SOAcc_l^m(i,j)^z = \sum_{z=1}^{L}\sum_{i=1}^{M}\sum_{k=1}^{N-1} Pr\left[\left[SOAcc_l(k-1) + \left(\sum_{X_l \in E_{tr}} \mathcal{F}_{l\leftarrow X_l}^{j(i)}(k) - \sum_{Y_l \in E_{tr}} \mathcal{F}_{l\rightarrow Y_l}^{j(i)}(k)\right) * \frac{\Delta k}{C_l}\right] \geq S_{min}\right] \geq \alpha_1 \tag{8}$$

Where $\alpha_1 \in [0,1]$ is the chance constraint factor as regards the lower pinch limit.

Similarly, the chance of violating the upper pinch limit (i.e. overcharging the BAT beyond 90% which can impact on the battery's lifetime and at worse damage the battery) is expressed as follows (9):

$$SOAcc_l^m(i,j)^z = \sum_{z=1}^{L}\sum_{i=1}^{M}\sum_{k=1}^{N-1} Pr\left[\left[SOAcc_l(k-1) + \left(\sum_{X_l \in E_{tr}} \mathcal{F}_{l\leftarrow X_l}^{j(i)}(k) - \sum_{Y_l \in E_{tr}} \mathcal{F}_{l\rightarrow Y_l}^{j(i)}(k)\right) * \frac{\Delta k}{C_l}\right] \geq S_{max}\right] \leq 1-\alpha_1 \quad (9)$$

Where $\alpha_2 \in [0,1]$ is the chance constraint factor of the upper pinch limit.

Thus, the probability density function (PDF) of $SOAcc_l^m$ can be analytically computed from the j^{th} column of the matrix, $MSOAcc_l^m$ and represented as follows in (10);

$$f_X(SOACC_l^m) = [f_{X_{11}}(SOAcc_l^m), f_{X_{12}}(SOAcc_l^m) \ldots, f_{X_{1N}}(SOAcc_l^m)] \quad (10)$$

Where, f_X denotes the PDF and subscript X indicates the dependent variable $SOAcc_l^m$.

Therefore, the desired operating range for $SOAcc_l^m\ (k)$ concerning the chance constraint is determined analytically with the cumulative distribution function (CDF) as follows in (11):

$$\int_{S_{min}}^{S_{max}} f_{SOAcc_l^m}(SOAcc_l^m)\, d(SOAcc_l^m) = F_{SOAcc_l^m}(S_{max}) - F_{SOAcc_l^m}(S_{min}) \quad (11)$$

Where, $F_{SOAcc_l^m}$ denotes the CDF of $SOAcc_l^m$ and the left-hand side of equation (11) is the PDF equivalent.

Therefore, the desired operating range for $SoAcc_{BAT}^m(k)$ for the chance constraint can be expressed in (12) as follows:

$$F^{-1}_{SOAcc_{BAT}^m}(\alpha_1) \leq F(SOAcc_{BAT}^m) \leq F^{-1}_{SOAcc_{BAT}^m}(1-\alpha_2) \quad (12)$$

Furthermore, to evaluate the probability of the $SOAcc_l^m$ violating the lower limit, the inverse CDF is utilised as follows in (13):

$$LSOAcc_l^m(k) = \sum_{k=1}^{N-2} inf\{F_{X_k}^{-1}(\alpha_1) < S_{min}\} \quad (13)$$

Where, $LSOAcc_l^m$ is a vector of n-elements, which represent point estimates of $SOAcc_l^m\ (k)$ that is less than the lower pinch chance constraint factor α_1 evaluated using the inverse CDF F_X^{-1}.

In addition, the MOES based on the probabilistic approach is determined as follows:

$If\ \exists\ \ LSOAcc_l^m < S_{min}$,

Then, the MOES; $\mathcal{F}_{BAT\leftarrow FC}^{POW} = (S_{min} - \arg\min[\, LSOAcc_l^m]) * C_l$ (14)

Thus, by activating the dispatchable resources (in this case the FC as shown in Figure 3(b)), the energy storage (such as BAT) is supplied with the MOES with an equivalent magnitude of flow $\mathcal{F}_{BAT\leftarrow FC}^{POW}$ as determined in (14) at present step k.

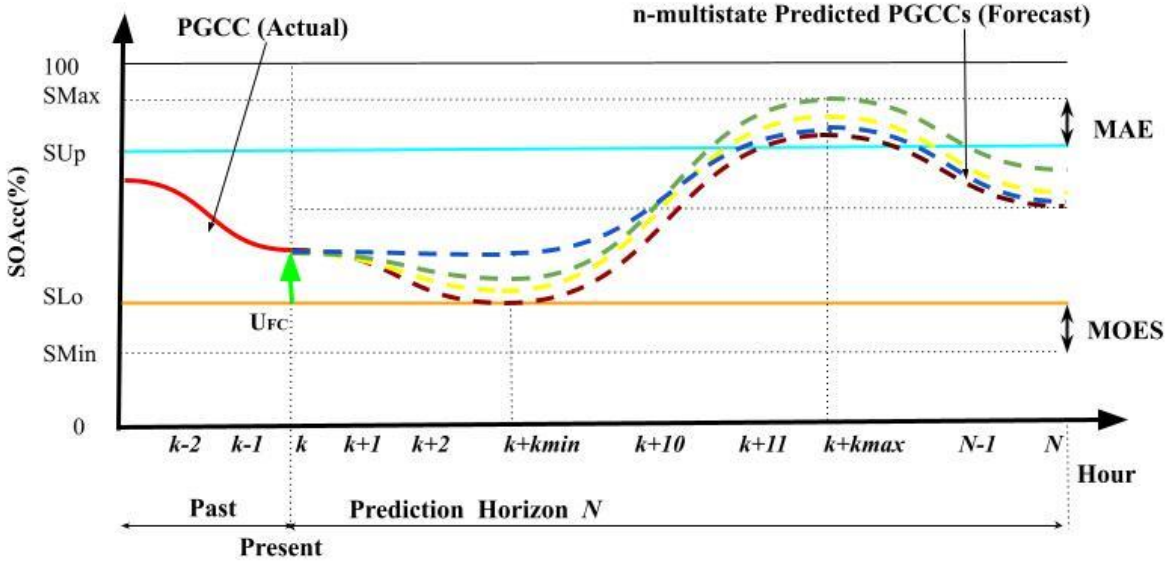

Fig. 3(b): Multistate PGCCs deficit energy matched with Fuel cell.

Similarly, after satisfying the lower pinch constraint, the PGCC is recomputed as in (9) and the violation of the upper pinch limit is determined as follows in (15):

$If\ \exists\ \ USOAcc_l^m(.) > S_{max}$

$$USOAcc_l^m(k) = \sum_{k=1}^{N-2} Sup\{F_{X_k}^{-1}(1-\alpha_2) > S_{max}\} \quad (15)$$

Where, $USOAcc_l^m$ is a vector of n-point estimates of $SOAcc_l^m\ (k)$ which are greater than the upper pinch chance constraint factor α_2 evaluated with the inverse CDF F_X^{-1}.

Consequently, the MAE is estimated from equation (15) to recover the excess energy (in this case an electrolyser in Figure 3(c)) which violates the upper operating limit as follows in (16):

$$\mathcal{F}_{BAT\rightarrow EL}^{POW} = (\arg\max[\, USOAcc_l^m] - S_{max}) * C_l \quad (16)$$

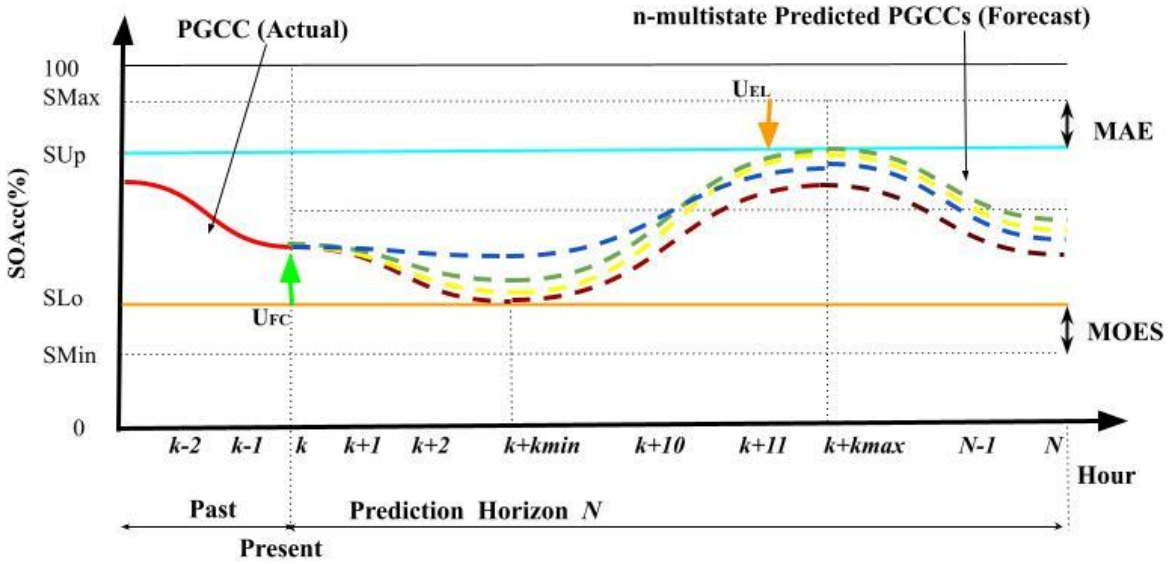

Fig. 3(c): Multistate PGCCs excess energy recovered with Electrolyser.

Thereafter, the AEEND for life cycle preservation is determined using the upper bound chance constraint to complete the PGCC shaping as follows in (17) and shown in Figure 3(d):

$$\text{AEEND: } U_c(k)=\begin{Bmatrix} \mathcal{F}_{BAT\leftarrow FC} & F_{X_k}^{-1}(1-\alpha_2) < SOAcc_{BAT}^{n}(k_1) \\ \mathcal{F}_{BAT\rightarrow EL} & F_{X_k}^{-1}(1-\alpha_2) > SOAcc_{BAT}^{n}(k_1) \\ 0 & Otherwise \end{Bmatrix} \forall_{k\in[N-1]} \quad (17)$$

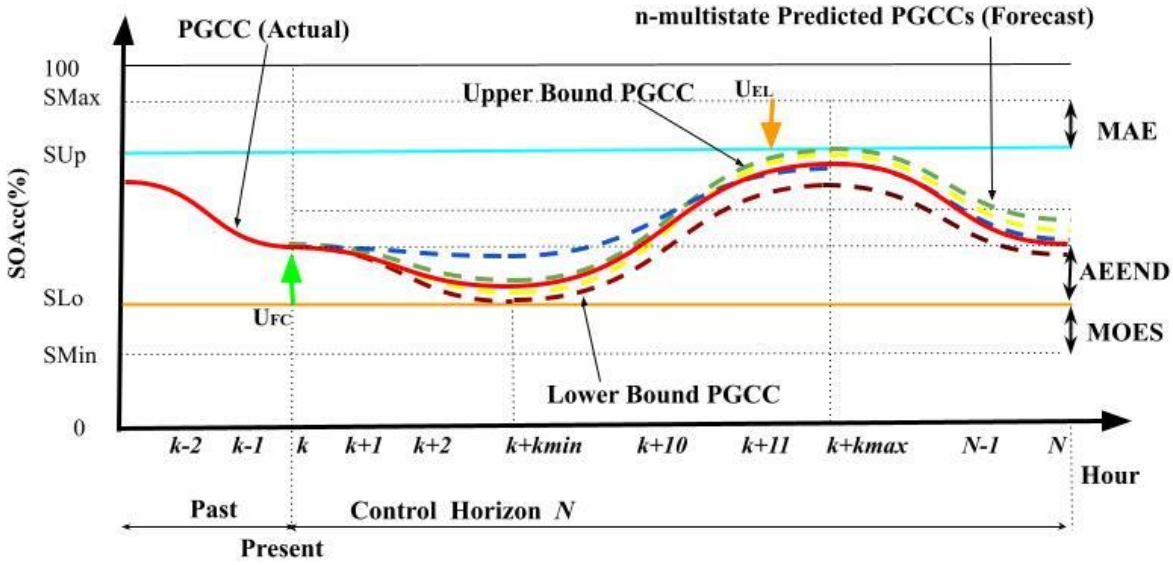

Fig 3(d): Complete shaping of the PGCC in the Control Horizon with Probabilistic Adaptive PoPA

The PoPA EMS decision-making variable $U_c(k)$ with the corresponding magnitude of energy flow determined in equations (14), (16) and (17) will satisfy both the lower and upper pinch points and AEEND, with regards to the chance constraint equations which have been formulated in a probabilistic adaptive receding horizon model predictive framework. Furthermore, the EMS sequence obtained with

the probabilistic model is therefore effected in the control horizon while considering the overall risk of violating the operational constraints. Figure 4, shows the P+Adaptive PoPA algorithm flowchart.

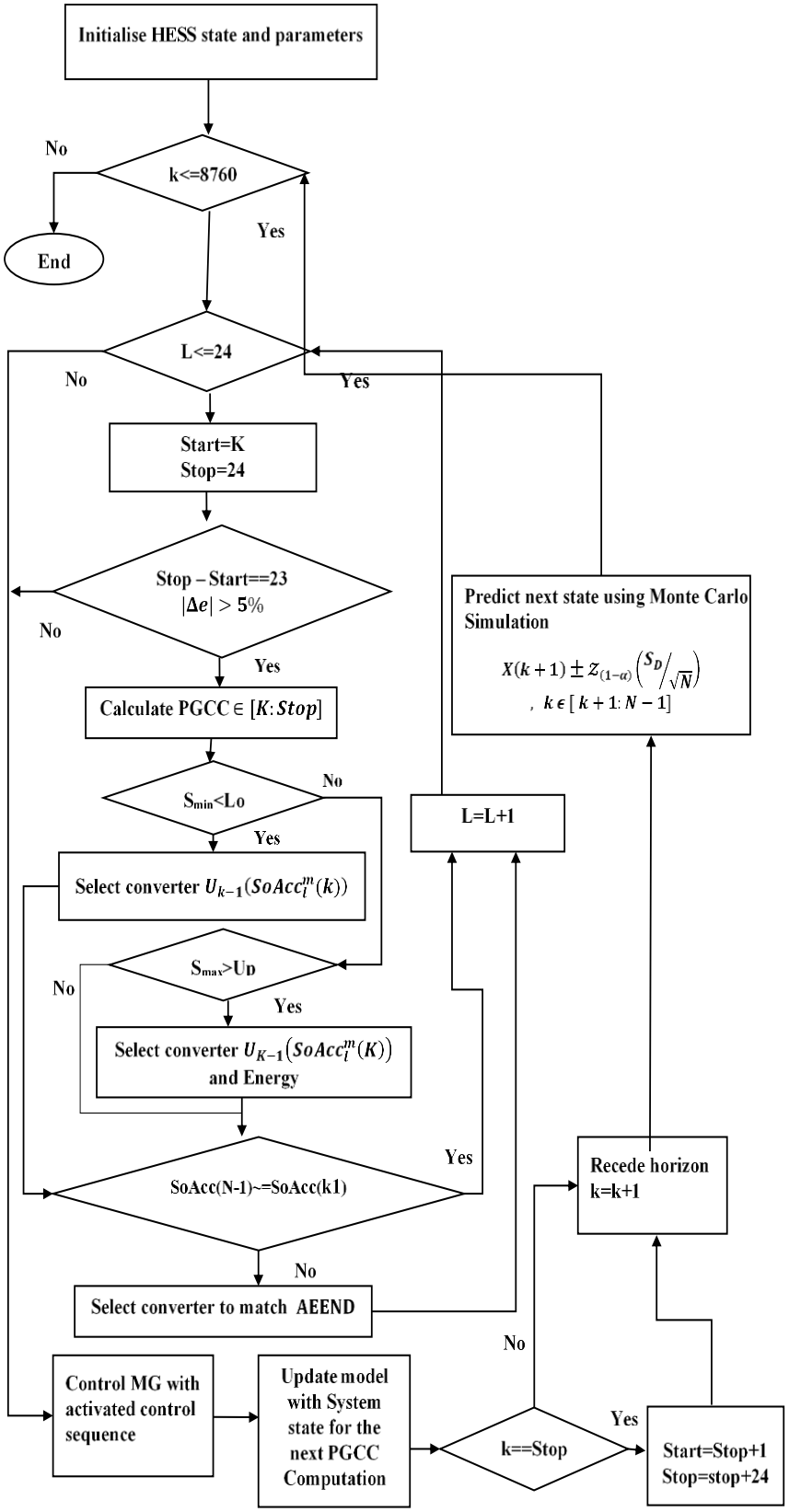

Fig. 4: Probabilistic+Adaptive PoPA Algorithm Flowchart

3.2 Recursive Least Square Probabilistic Adaptive PoPA

To improve the estimation of actual $SOAcc^n$ via the probabilistic PoPA, a simple correction factor that minimises the residual error loss function between the actual $SOAcc^n$ and estimated $SOAcc^m$ can be incorporated recursively into the process.

Let the equilibrium relationship between the actual $SOAcc^n$, the estimated $SOAcc^m$ and an unbiased multiplicative correction factor X_{cf} be:

$$SOAcc^n(k) = SOAcc^m(k) * X_{cf} \tag{18}$$

Where,

$$SOAcc^m(k|) = \frac{[LSOAcc^m(k) + USOAcc^m(k)]}{2} \tag{19}$$

Such that, $SOAcc^m(k)$ is the expectation of respectively are the lower and upper bound confidence intervals (of say 98%) on the expected value, and X_{cf} is the multiplicative correction factor. Thus, by the ordinary least square error method [60-62], the unbiased residual error correction factor X_{cf} is determined via a mean squared error (MSE) loss function in equations (20) – (23) as follows:

$$MSE = \frac{1}{2N}\sum_{k=1}^{N}(SOAcc^n(k) - SOAcc^m(k) * X_{cf})^2\,\Delta k \tag{20}$$

Taking the derivative of MSE Error denoted as E, w.r.t, X_{cf}:

$$\frac{d(MSE)}{d(X_{cf})} = -\frac{1}{N}\sum_{k=1}^{N}(SOAcc^n(k) - SOAcc^m(k) * X_{cf})SOAcc^m(k) \tag{21}$$

Decomposing the right-hand side of the equation:

$$\frac{1}{N}\sum_{k=1}^{N}(SOAcc^n(k) * SOAcc^m(k) - \frac{X_{cf}}{N}\sum_{k=1}^{N}(SOAcc^m(k))^2 = 0 \tag{22}$$

Therefore, the correction factor X_{cf}, is expressed:

$$X_{cf} = \frac{\sum_{k=1}^{N}(SOAcc^n(k) * SOAcc^m(k)}{\sum_{k=1}^{N}(SOAcc^m(k))^2} \tag{23}$$

Thus, X_{cf} is a least-square solution that minimises the residual error function in equation (23).

Furthermore, equation (23) is decomposed into a recursive formulation to form an online correction factor with X_{cf} in equations (24)-(28) as follows:

Let, ${X_{cf}}^k$ be the normalised cumulative correction factor at current time $k = 1{:}\,N$,

$$X_{cf}{}^{k} = \frac{\sum_{k=1}^{N}(SOAcc^{n}(k) * SOAcc^{m}(k)}{\sum_{k=1}^{N}(SOAcc^{m}(k))^{2}} \tag{24}$$

And $X_{cf}{}^{k-1}$ is the normalised cumulative correction factor at the previous time step $k = 1{:}\,N-1$,

$$X_{cf}{}^{k-1} = \frac{\sum_{k=1}^{N-1}(SOAcc^{n}(k) * SOAcc^{m}(k)}{\sum_{k=1}^{N-1}(SOAcc^{m}(k))^{2}} \tag{25}$$

While $X_{cf}{}^{*}$, is the correction factor at time step k only,

$$X_{cf}{}^{*} = \frac{(SOAcc^{n}(k) * SOAcc^{m}(k))}{(SOAcc^{m}(k))^{2}} \tag{26}$$

The recursive form of the correction factor is thus,

$$X_{cf}{}^{k} = [(N-1)X_{cf}{}^{k} + X_{cf}{}^{*}]/N \tag{27}$$

$$X_{cf}{}^{k} = X_{cf}{}^{k-1} + \left[X_{cf}{}^{*} - X_{cf}{}^{k-1}\right]/N \qquad \forall\, k = 1{:}\,N \tag{28}$$

Therefore, for all real values of $SOAcc^{n}$ greater than zero, the optimal value of the error correction term is 1, if the prediction of $SOAcc^{m}$ is accurate (i.e. error is 0), and less than or greater than 1, if the error between the actual and predicted SOAcc is positive or negative respectively. Consequently, $X_{cf}{}^{k}$ is 1 at initialisation. Furthermore, in the MATLAB environment, the regression fitting toolbox is used to fit a simple linear model $y = Ax + B$ in the same manner as presented in this section for the sake of comparison. Thus, the probabilistic adaptive PoPA fitted with the least-square error is denoted as RLS+P PoPA ($y = Ax$), and RLS+P PoPA ($y = Ax + B$), where B in the later model is the bias and A is the multiplicative factor.

3.3 Load demand and Weather Data

The historical household load demand profile is shown in Figure 5, with a peak load of 2.08 KW and a 10KWh peak solar irradiance data shown in Figure 6, corresponding to 54.9783° N, 1.6178° W, are obtained from [63] and [64] respectively. The load profile data set consists of the aggregated power demand of uncontrollable appliances at each hourly time interval representing the consumer's usage pattern. The historical load profile data set, $A\ (i, j)$ obtained over 365 days, at each hourly time step k, such that i=1, 2, 3…365 is partitioned into disjointed groups of $A(i,k) = \{A_1, A_2, A_3, A_4\}$ which forms the LD distribution $F_X LD^{i}(k)$. Each group of load demand data set distinctly corresponds to the consumer's power usage pattern correlating to the four seasons in a year [65]. Therefore, from the consumer's historical energy consumption profile (with average load plotted in red) as shown in Figure 5, a probability distribution $F_X LD^{i}(k)$ is easily realised.

In the Monte Carlo simulation, the load demands in each cluster (for each i at time step k) are assumed to be normally distributed [66]. Furthermore, in other to validate the proposed approach, the actual load is randomly selected with uniform probability from the load demand distribution corresponding to the time instance (k). Typically, as shown in Figure 2.3, the historical load profile for Q1 has a dual peak characteristic, which mostly peaks on noonday and during the late evening. Specifically, as shown in Figure 5, the historical load profile for Q1 has a dual peak characteristic, which mostly peaks at noonday and during the late evening period. Similarly, the uncertainty in the solar irradiance can be realised as a Gaussian distribution $\mathcal{N}(0, \sigma = 20)$ or consequently as any type of distribution within the presented procedure.

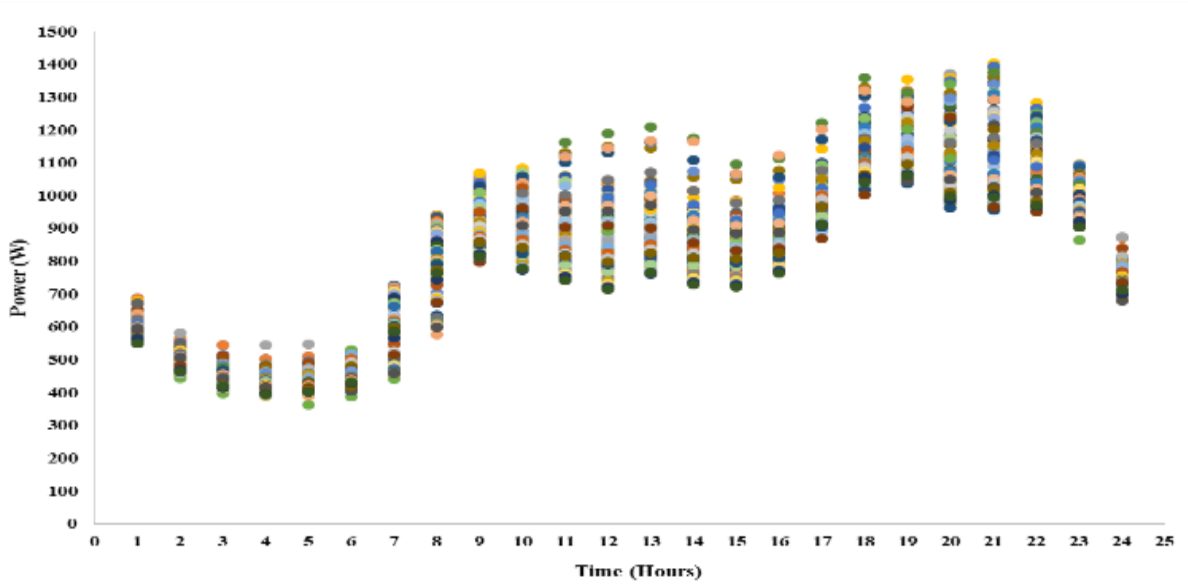

Fig. 5: Load demand profile showing energy consumption pattern variability during winter [63].

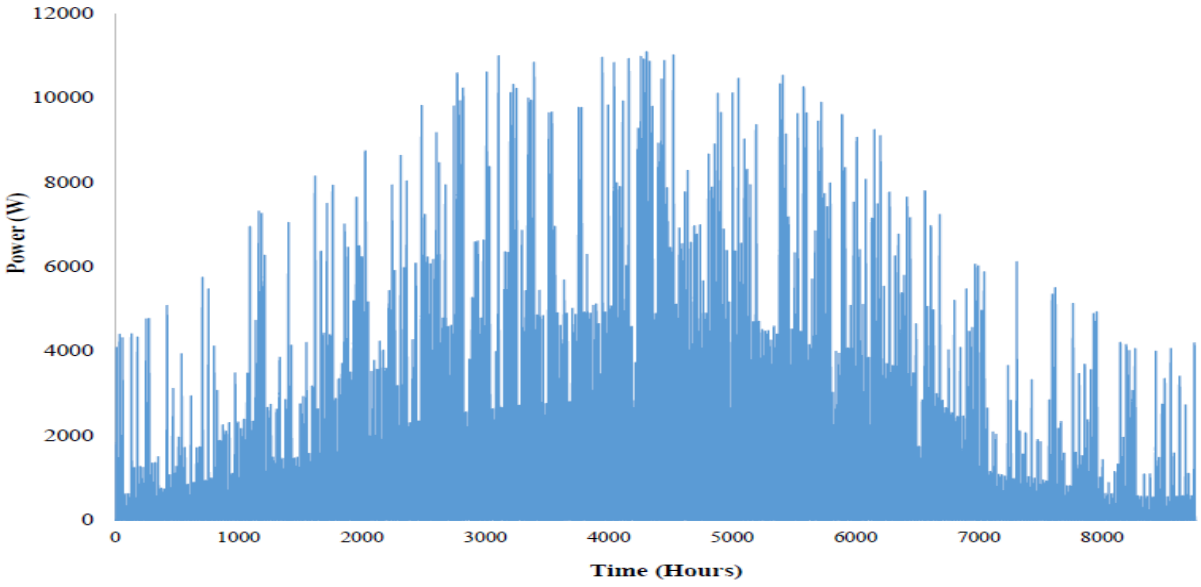

Fig. 6: PV Energy Profile for 8760h [64].

The histograms of the first quarterly load consumption variability from historical data is shown in Figure 7, for each hour, k in winter (Q1). The histograms fundamentally depict Weibull, bimodal and normally distributed load demand profiles. Furthermore, Table 1, conveys the statistical information of the quarterly Load profiles with Q1 exhibiting the most significant uncertainty in contrast to the other seasons. Furthermore, the histogram for summer (Q2), spring (Q3) and autumn (Q4) respectively are shown in Figures A1 to A3 in the appendices. Precisely, as seen in Table 1, during Q1, the uncertainty peaked at noon with a magnitude of 30.2% and thereafter, at 20:00h with a magnitude of 27.9%. Similarly, as shown in Table A1 in the appendices, the largest uncertainty occurred at 13:00h, with a magnitude of 8.5% in Q2. Furthermore, as depicted in Table A1 to A3 in the appendix, the highest uncertainty was recorded during the periods of 14:00h and 13:00h during Q3 and Q4, respectively. Thus, the load demand uncertainty mainly depicts both daily and seasonal variation patterns.

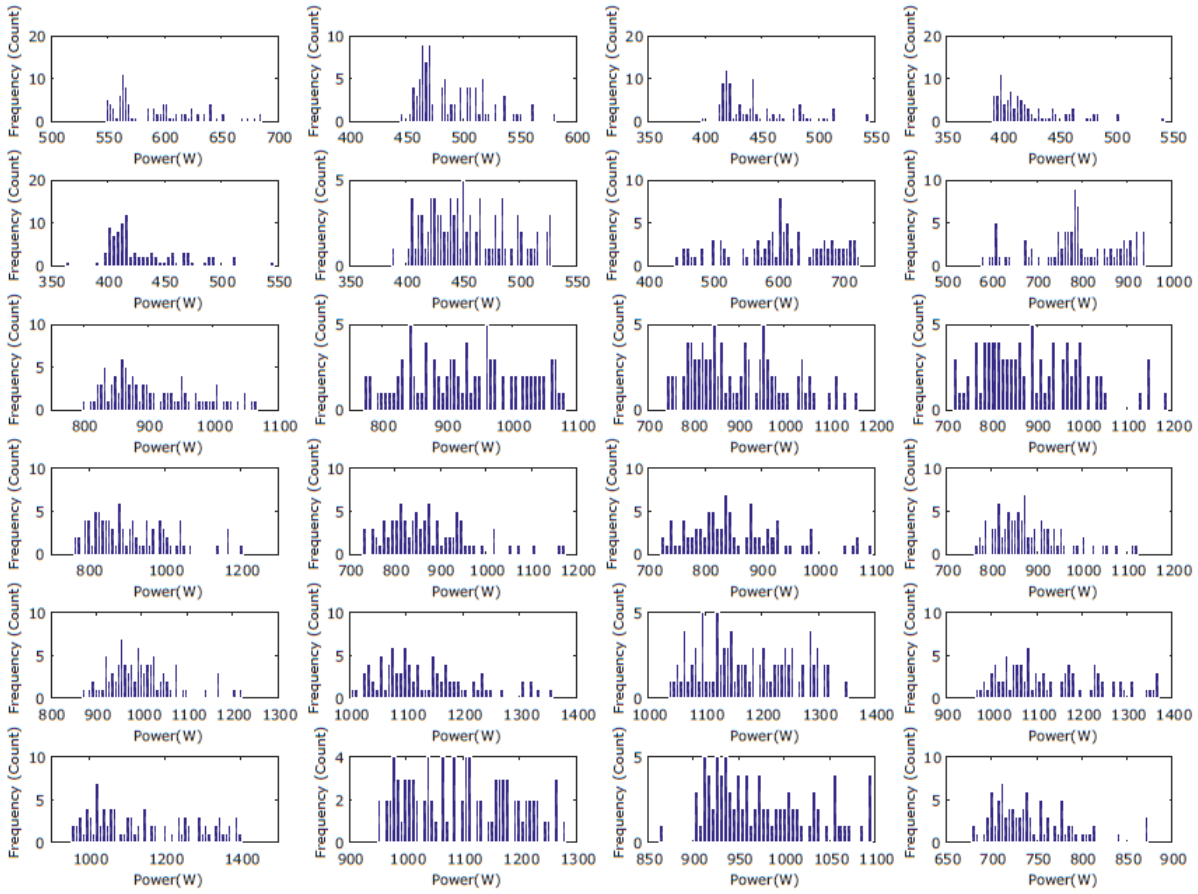

Fig. 7: Histogram plot for the hourly daily load distribution in Q1

Table 1: Statistical central tendencies in First Quarter (Winter) Load demand profiles

FIRST QUARTER (WINTER)					
HOUR	MIN	MEAN	MAX	STD DEV.	UNCERTAINTY (%)
1	337.5	506.5	685.9	99.5	20
2	219.1	392.5	582.0	101.9	26
3	182.0	355.6	544.4	102.0	29
4	137.4	323.0	543.0	109.08	34
5	161.6	338.3	546.8	103.8	30
6	388.4	453.4	528.1	38.8	9
7	561.5	633.7	726.4	40.2	6
8	668.4	792.6	940.0	76.6	10
9	517.9	788.1	1068.0	158.8	20
10	637.1	849.3	1083.3	125.0	15
11	456.8	749.4	1129.4	173.1	23
12	334.5	686.3	1148.3	207.9	30
13	436.3	738.5	1144.0	179.0	24
14	470.5	724.3	1056.3	150.6	20
15	304.1	642.9	1048.0	199.8	30
16	395.4	698.4	1076.1	178.9	26
17	809.4	949.3	1168.1	83.7	9
18	825.3	1043.2	1329.6	129.1	12
19	981.1	1147.9	1352.2	98.6	9
20	489.2	932.6	1370.9	260.4	28
21	980.7	1177.6	1403.6	116.8	10
22	878.2	1070.3	1280.9	113.1	11
23	727.4	910.2	1096.2	107.5	12
24	332.5	593.0	873.3	153.2	26

4. Results and Discussion

4.1 Monte Carlo Simulation with the probabilistic Adaptive PoPA

The proposed method utilising the chance-constrained power pinch for energy management is simulated in MATLAB based on N-samples randomly generated from a uniform distribution A(i,k). In the Monte Carlo simulation, the resulting load demands sampled randomly from the kernel density estimation (KDE) [67] distribution in each cluster (for each i at time step k) are assumed to be normally distributed, since the samples are sufficiently or approximately large (i=1000) enough to support convergence by the central limit theorem [68-70]. The chance constraints factors were both set to 1% during the simulation. Therefore, the state of charge of the battery has a 98% probability of operating within the optimal region (30% $\leq SOAccn\ ^{n}_{BAT} \leq$ 90%) as illustrated by point 4, in Figure 8. The red line is the CDF, and the blue is an equivalent PDF plot, while the dotted black lines represent quantiles corresponding to the chance constraints. A summary of the stages in the realisation of the Probabilistic Adaptive PoPA EMS is graphically illustrated in Figure 8.

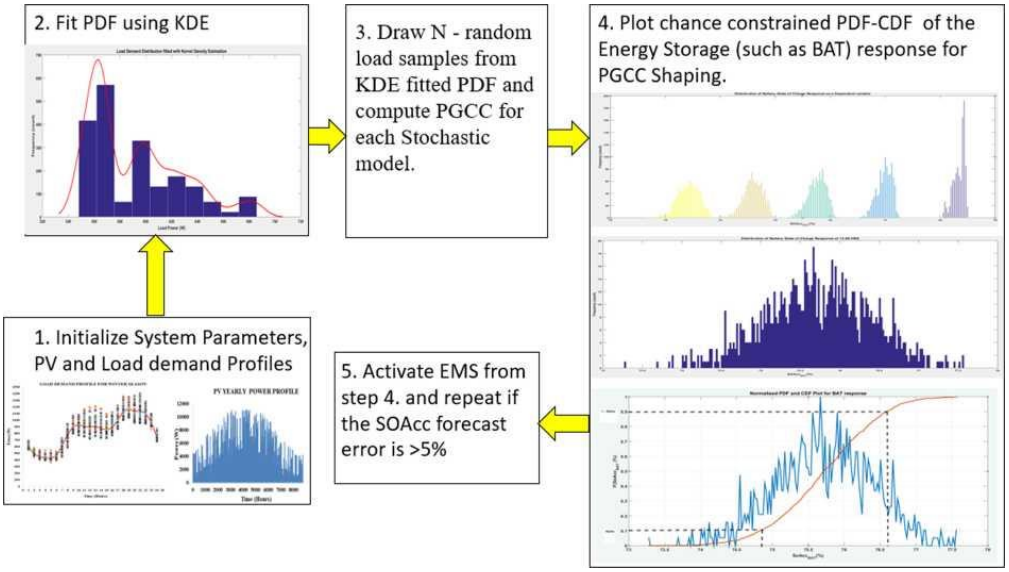

Fig. 8: Illustration of the Probabilistic+Adaptive PoPA EMS

The parameters of the HESS in Table 2, used as an experimental case study is obtained from a real system in [7], with real residential load demand profiles of a typical British home sourced from ELEXON [63] with solar irradiance data for Newcastle, United Kingdom sourced from NREL [64].

Table 2: HESS Micro-grid parameters [7]

System Components	Specification
Load (peak)	2080 W [63]
PV (66.64 W rated power)	150 [64]
DSL	2210 W
BAT	3000 Ah / 48 V
FC	3000 W
EL	4000 W
HT	30 bar, 15 m^3
$\eta_{CV},\eta_{PV},\eta_{FC},\eta_{EL}$	0.95, 0.10, 0.87, 0.87

4.2 Uncertainty Analysis of the Probabilistic Adaptive Algorithms

The performance of the proposed three probabilistic methods; P+Adaptive PoPA, RLS+P PoPA with/without bias ($y = Ax + B$ and $y = Ax$ respectively) are compared against the Day-ahead, Adaptive and Kalman+Adaptive PoPA EMSs presented in [27]. The comparison is evaluated over an operational period of 72h (short term) and 8760h (long term). For the sake of consistency in comparing the proposed methods to existing methods in previous work, the initialisation settings for the $SOAcc_l^m$ is such that $l \in \{\text{BAT, HT and WT}\}$ corresponds to 70%, 80% and 30% respectively.. Similarly, the same properties of the non-Gaussian (Bimodal distribution) and Gaussian load demand used in [27] are used to project the uncertainty dynamics here for uniformity and consistency.

The performance indices expressed in (29) - (31) for EM evaluation is for the total number of times the S_{Lo}^{l} (30%) and S_{Up}^{l} (90%) Pinch limits are violated and the DSL activated [27];

$$\text{Sum of Deficit}=\sum_{k=1}^{N=8760}\begin{Bmatrix}1 & S_{Lo}^{l} > SOAcc_{BAT}^{n}(k)\\ 0 & otherwise\end{Bmatrix} \quad (29)$$

$$\text{Sum of Surplus}=\sum_{k=1}^{N=8760}\begin{Bmatrix}1 & S_{Up}^{l} > SOAcc_{BAT}^{n}(k)\\ 0 & otherwise\end{Bmatrix} \quad (30)$$

$$\text{Sum of DSL activation}=\sum_{k=1}^{N=8760}\begin{Bmatrix}1 & 20\% > SOAcc_{BAT}^{n}(k)\\ 0 & otherwise\end{Bmatrix} \quad (31)$$

4.2.1 Short Term Analysis under Non-Gaussian Uncertainty

The proposed P+Adaptive PoPA method utilising the chance-constrained power pinch for energy management is simulated in MATLAB based on N-samples randomly generated from a uniform distribution $A(i,k)$. The chance constraints factors were both set to 1% during the simulation. Therefore, the state of charge of the battery has a 98% probability of operating within the optimal region ($30\% \leq SOAcc_{BAT}^{n} \leq 90\%$) as illustrated in Figure 6. The red line is the CDF and the blue is an equivalent PDF plot, while the black lines represent quantiles corresponding to the chance constraints. Furthermore, as shown in Figure 7, the systems PGCC is bounded, by both the probabilistic lower and upper PGCC. The response of the system throughout 72 hrs is shown in Figure 9. The red and blue lines in Figure 9, are the lower and upper predicted PGCC based on the chance constraint. The yellow dashed line represents the actual response of the system. The PGCC upper pinch violation at 40th hr accurately predicts the pinch during the first 72 hrs hence the EL is activated.

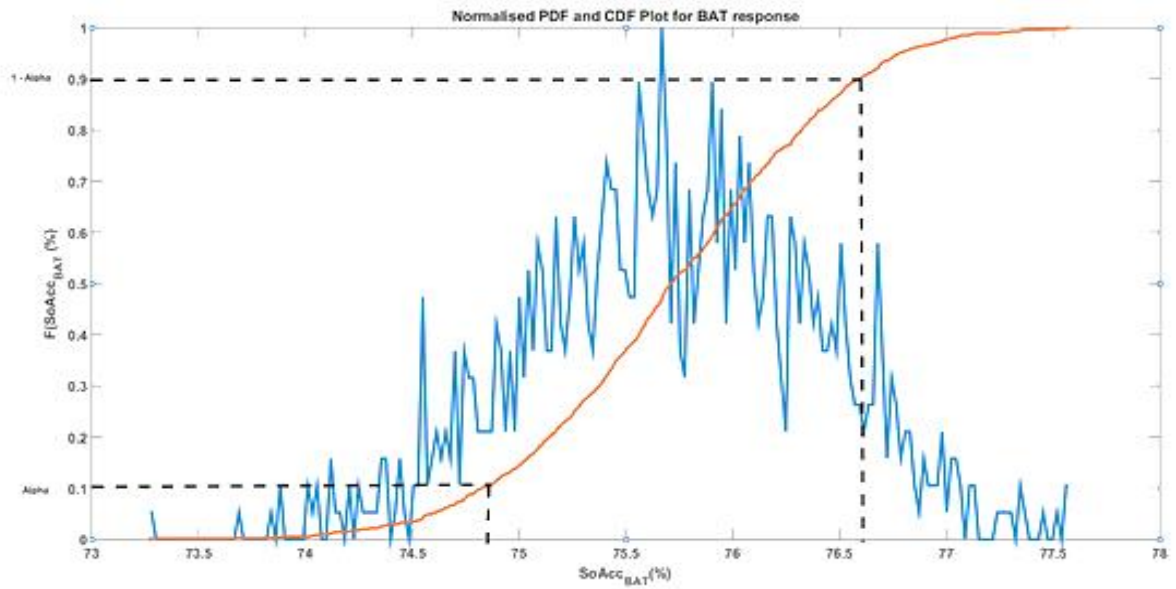

Fig. 9: P+Adaptive PoPA CDF-PDF Quantile plot of the $SOAcc_{BAT}$ PGCC evaluated at 1h.

As shown in Figure 10, the actual PGCC is bounded by both the probabilistic lower and upper PGCC based on a 98% chance of violating the SLo and SUp pinch utility under non-Gaussian uncertainty. The upper and lower predicted PGCC bounds are shown as the red and blue plots in Figure 10, while the actual PGCC is indicated by the yellow dashed line. The operational constraints were never violated by the P+Adaptive PoPA. Nevertheless, as seen in Figure 11, the FC and EL were activated 6 and 3 times, respectively and the corresponding HT and WT response over 72h with the P+Adaptive PoPA is shown in Figure 12.

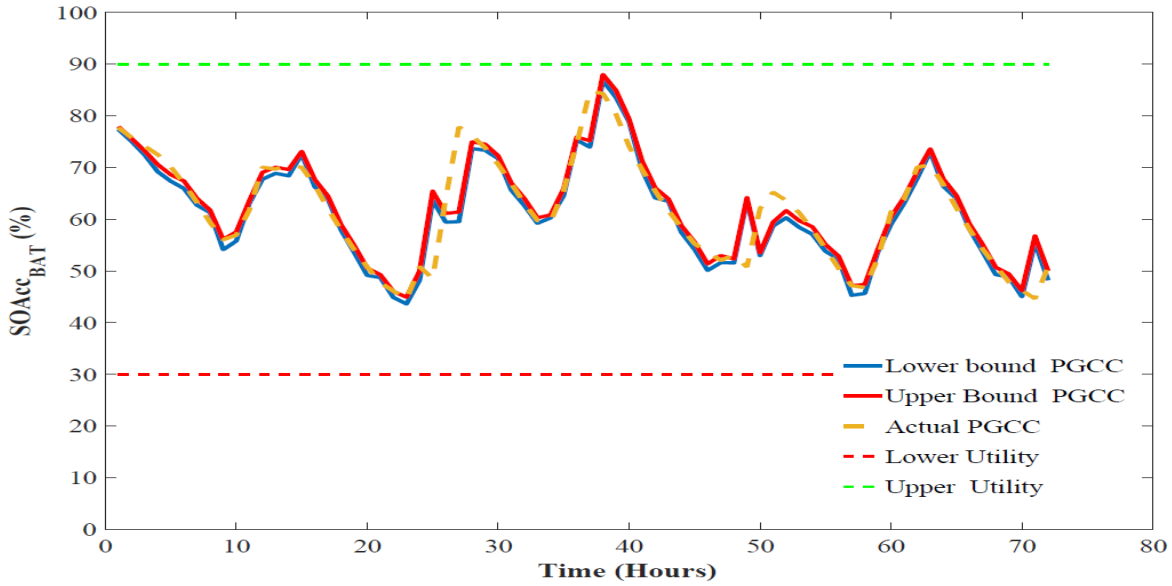

Fig. 10: Response of the Battery's state of charge to P+Adaptive PoPA

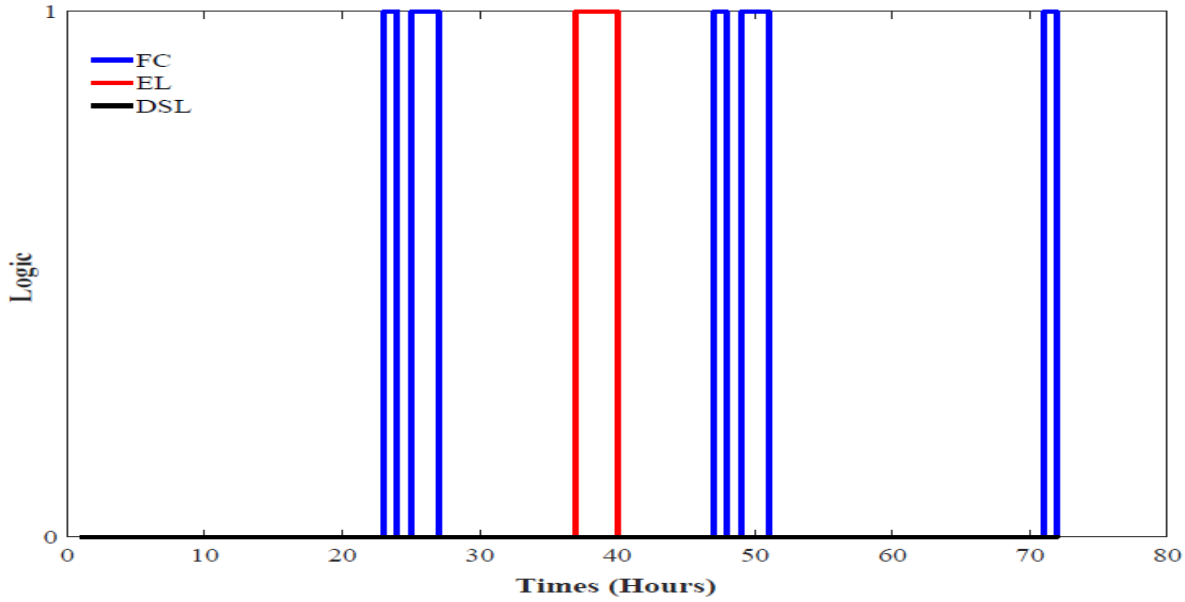

Fig. 11: P+Adaptive PoPA converter logic over 72h

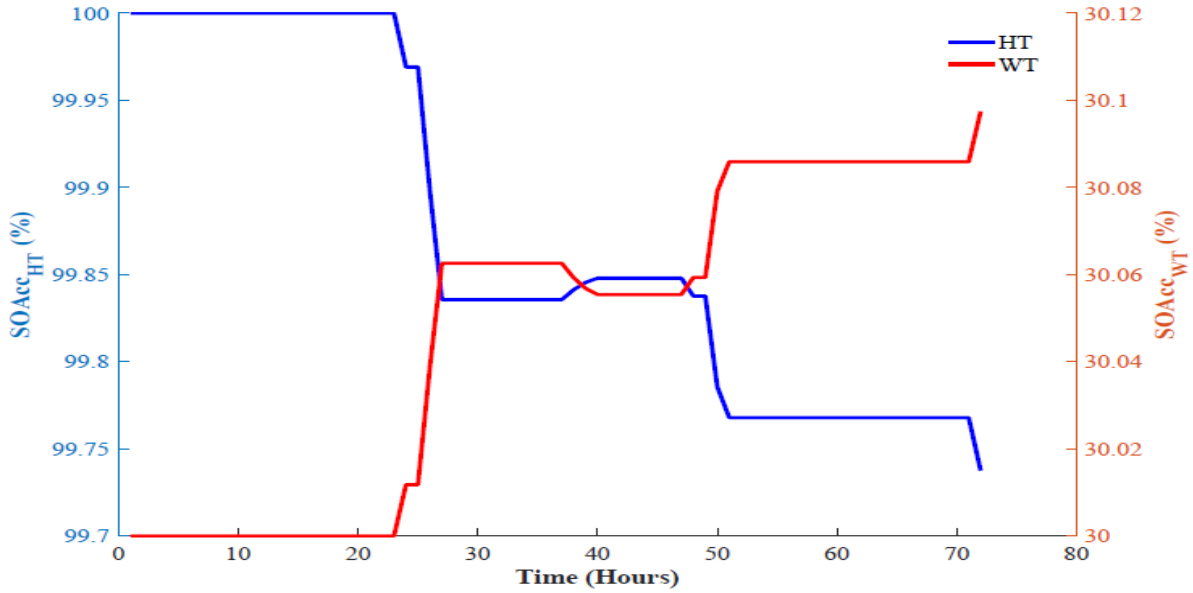

Fig. 12: P+Adaptive PoPA HT and WT response over 72h

Similarly, the RLS+P PoPA with and without the bias also recorded no violations concerning the SLo and SUp pinch utility as shown in Figures 13 and 16 respectively. Nevertheless, while, RLS+P PoPA without bias activated the FC 7 times and the EL 3 times as shown in Figure 14, with the RLS-P PoPA with the bias, the activation of the FC and EL increased to 8 and 5 times respectively as shown in Figure 14. Hence, an increase in operational cost or resources with a probabilistic PoPA approach, particularly with an increase in the complexity of the residual error regression model is a trade-off for robustness. The HT and WT response of the P+Adaptive, the RLS-P without bias and with bias are shown in Figures 15 and 18, respectively. The performances are presented in Table 3.

It is important to note that the DA, Adaptive, Kalman, RL+Adaptive, P+Adaptive, RLS-P($y = Ax$), and RLS-P ($y = Ax + B$) PoPA EMS are referred to as methods M1-7 respectively in Tables 3 to 8, for conciseness.

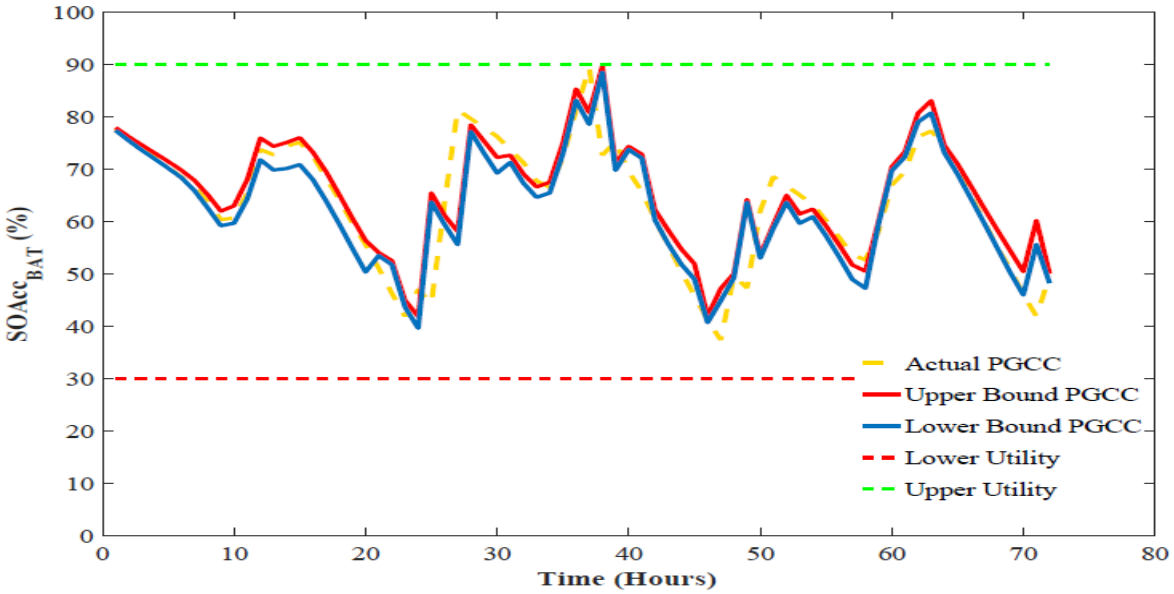

Fig. 13: Performance of the RLS-P PoPA ($y = Ax$) strategy over 72h

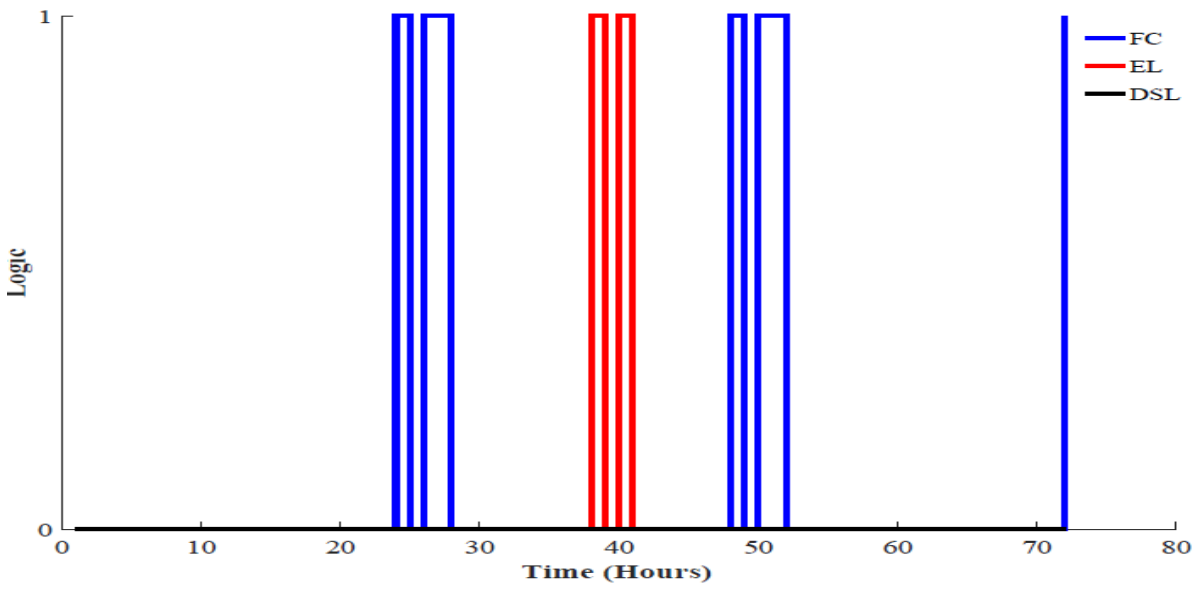

Fig. 14: RLS-P PoPA ($y = Ax$) converter logic over 72h

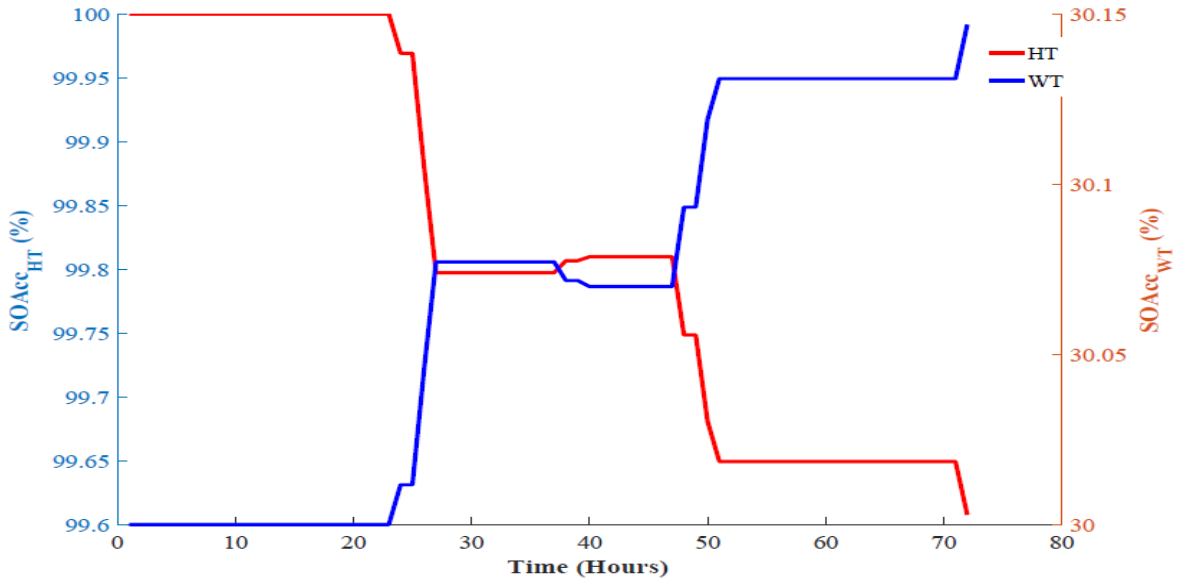

Fig. 15: RLS-P PoPA ($y = Ax$) HT and WT response over 72h

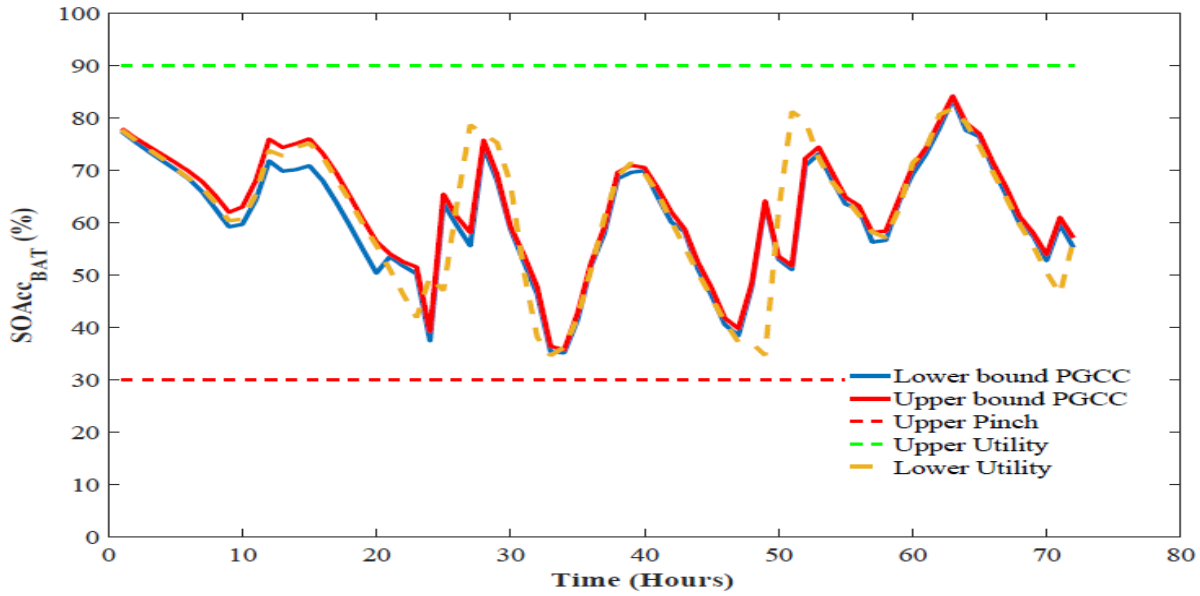

Fig. 16: Performance of the RLS-P PoPA ($y = Ax + B$) strategy over 72h

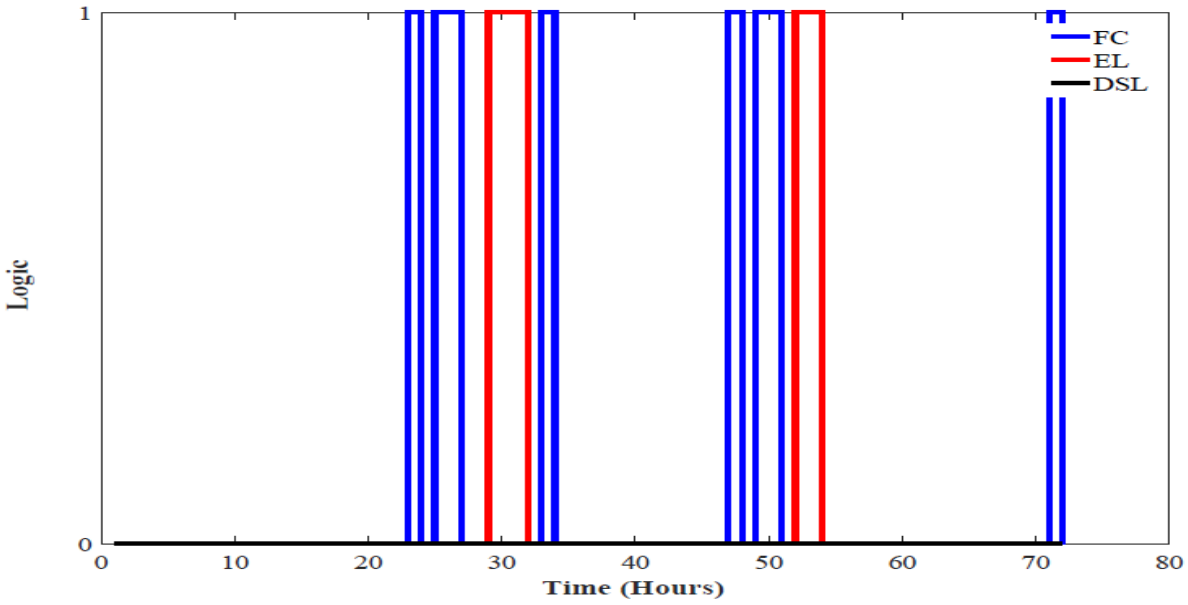

Fig. 17: RLS-P PoPA ($y = Ax + B$) converter logic over 72h

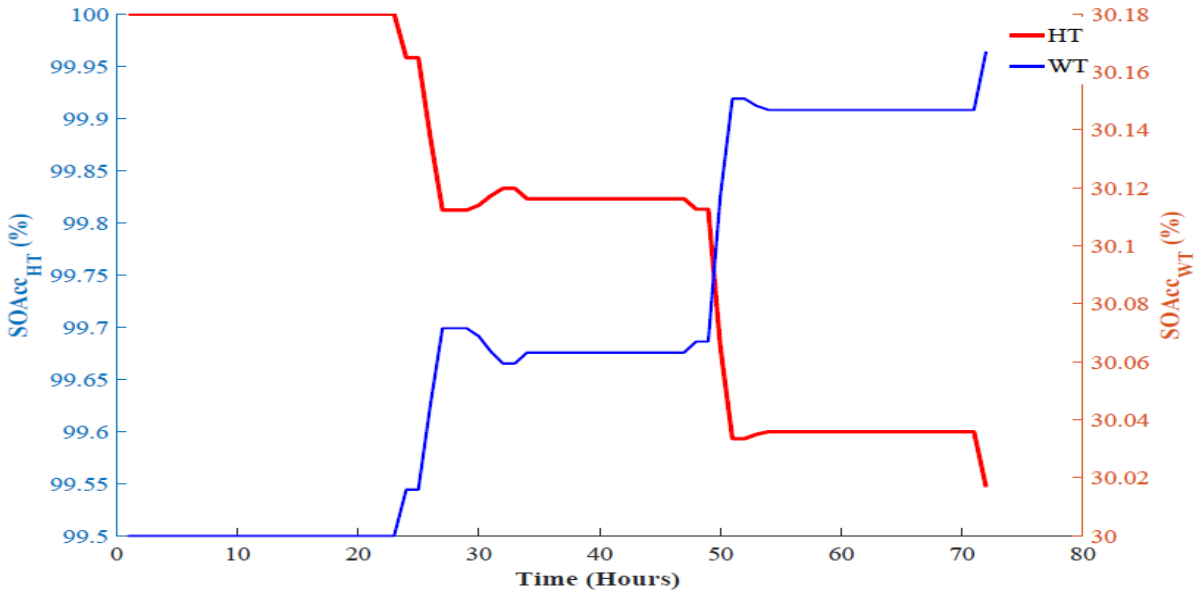

Fig. 18: RLS-P PoPA ($y = Ax + B$) HT and WT response over 72h

Table 3: Summary of performance of EMS methods under Non-Gaussian Uncertainty over 72h

Operational parameters	**PoPA EMS**						
	M1	**M2**	**M3**	**M4**	**M5**	**M6**	**M7**
Lower Pinch violation ($SOAcc_{BAT}^{n}$ < 30%)	14	7	7	1	0	0	0
Upper Pinch violation ($SOAcc_{BAT}^{n}$>90%)	0	0	0	0	0	0	0
DSL Activation	2	0	0	0	0	0	0

4.2.2 Short Term Analysis under Gaussian Uncertainty

Similarly, under the Gaussian uncertainty case study, the RLS+PoPA with the simple correction factor (i.e. without the bias), violated the SUp once, while the P+Adaptive, RLS+Adaptive with bias as shown in Table 4. Nevertheless, in contrast to the DA and Adaptive PoPA which had 13 and 3 violations of the SLo, the P+Adaptive, RLS+PoPA without bias, Kalman+Adaptive PoPA had none. Accounting for robustness and accuracy results in an increased frequency of FC and EL activation cycles and consequently incur losses, further increasing the operating cost with the simple least-squares mechanism aimed at minimising the mean squared error between the actual SOAccn_{BAT}^{n} and estimated SOAccn_{BAT}^{m} from the MCS process. Nevertheless, further investigation using a long term (8760h) scenario case study will be presented.

Table 4: Summary of performance of EMS methods under Gaussian Uncertainty algorithms over 72h.

Operational parameters	PoPA EMS						
	M1	M2	M3	M4	M5	M6	M7
Lower Pinch violation ($SOAcc_{BAT}^{n}$ < 30%)	13	3	0	0	0	0	0
Upper Pinch violation ($SOAcc_{BAT}^{n}$>90%)	0	0	0	0	0	1	0
DSL Activation	0	0	0	0	0	0	0

4.2.3 Long term under Non-Gaussian uncertainty

P+Adaptive PoPA

The probabilistic approach P+Adaptive PoPA which violated the SLo and SUp 321 and 828 times as shown in Figures 19 and 20, was only better in performance than the RLS+P ($y = Ax + B$) concerning the SUp and DA-PoPA concerning the SLo indices. The DSL, FC and EL were activated by the P+Adaptive PoPA EMS 126, 1935, and 926 times respectively, as shown in Table 5. Therefore, the consequence of the P+Adaptive PoPA using the FC robustly to maintain the PGCC bound led to premature exhaustion of the H2 in the HT as the $SOAcc_{HT}$ dipped below 10% at 7500 h, as seen in Figure 21. Consequently, the FC become unavailable for dispatch at 7500h. Nevertheless, as shown in Figure 19, the P+Adaptive PoPA showed sensitivity in curtailing the excessive overcharging of the BAT. Furthermore, the probability of violating the SUp had a steep rise even in the months of poor sunshine and even so steeper in the periods of peak sunshine, as shown in Figure 21. Therefore, an adaptive mechanism to correct the prior distribution should suffice as this would adjust the prior distribution or the estimated PGCC bound based on the residual error to match the reality.

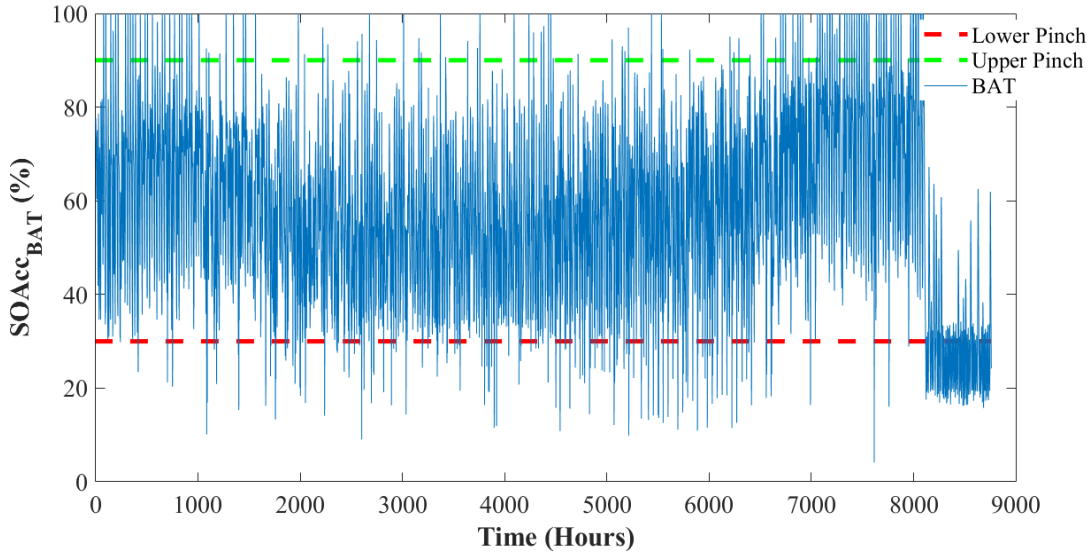

Fig. 19: 8760h BAT response with P+Adaptive PoPA

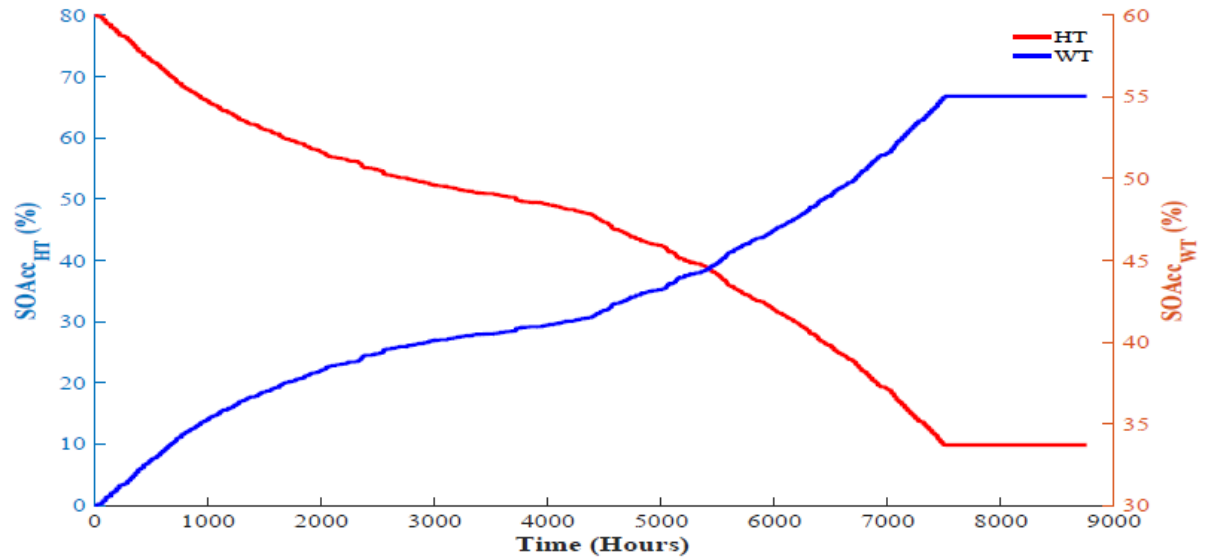

Fig. 20: HT and WT response for 8760h with P+Adaptive PoPA

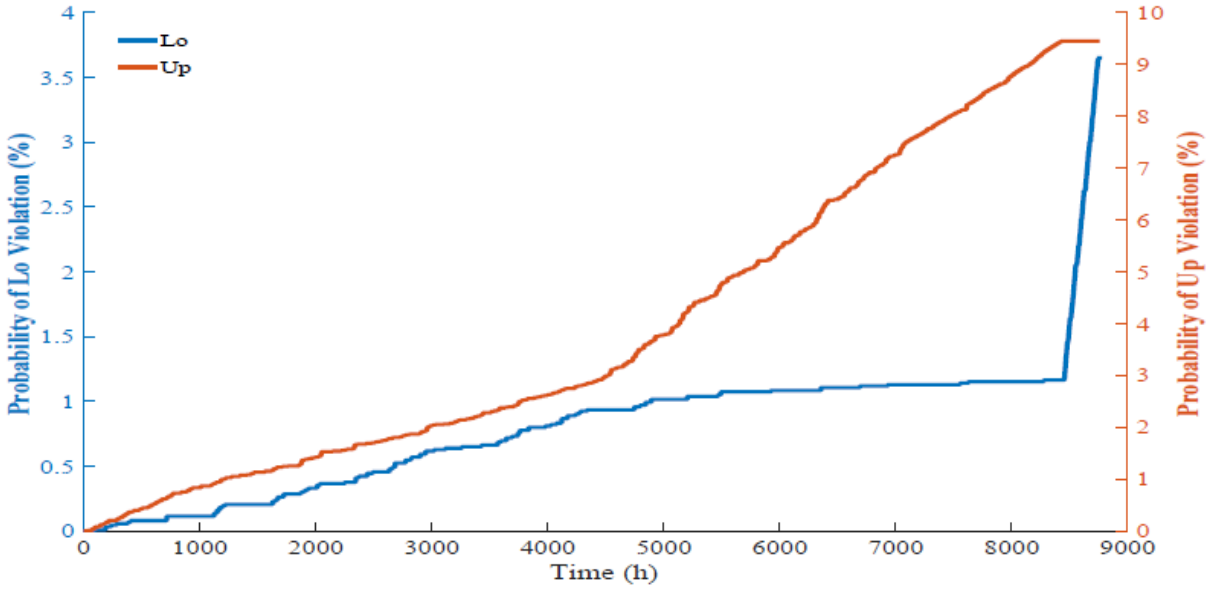

Fig. 21: Probability of violating the upper and lower limits of BAT in 8760h with P+Adaptive PoPA

RLS+P PoPA (y=Ax)

In Table 5, the RLS+P is shown to have had an enhanced performance compared to the P+RLS as the SLo which was violated 198 times and SUp 666 times amounted to a 15% and 20% reduction respectively. The response of the BAT over 8760 h is shown in Figure 22. Consequently, despite a 75% reduction in the SLo violation, the SUp violation only improved by 12% against the performance of the DA-PoPA. Nevertheless, the improvement is a result of the residual error correction factor, which was based on the simplest linear model $y = Ax$. Again, with the RLS+P ($y = Ax$) PoPA, the effect of the

robust bound led to the accelerated exhaustion of the H2 as shown in Figure 23 only after which the violation of the SLo had a steep rise from 2.2% to 7% as shown in Figure 24.

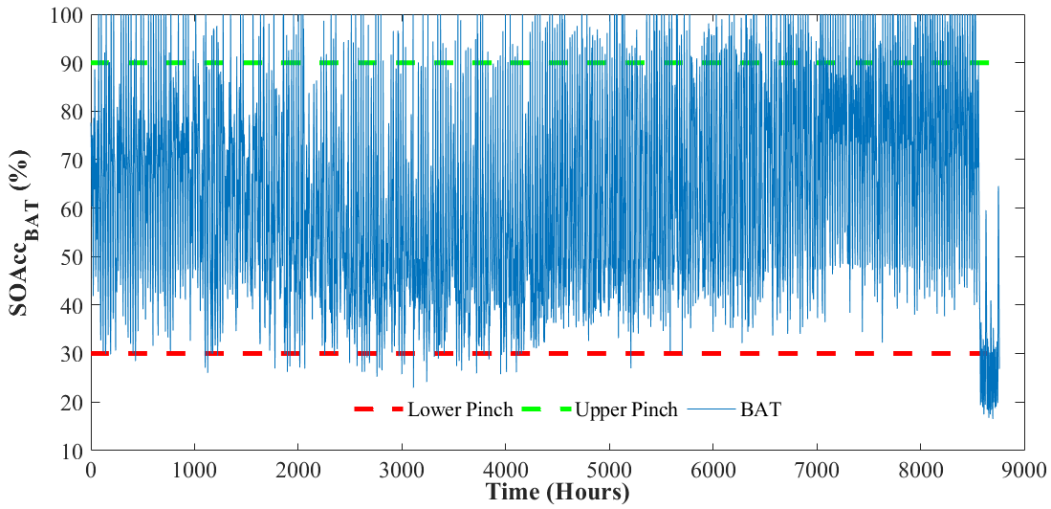

Fig. 22: 8760h BAT response with RLS+P PoPA

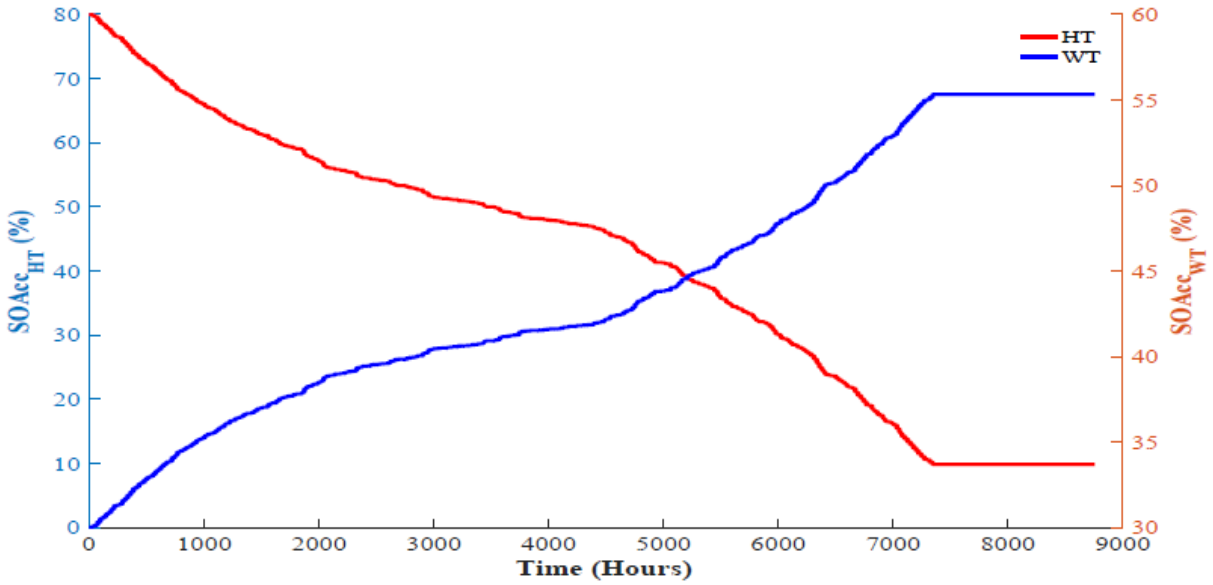

Fig. 23: HT and WT response for 8760h with RLS+P PoPA

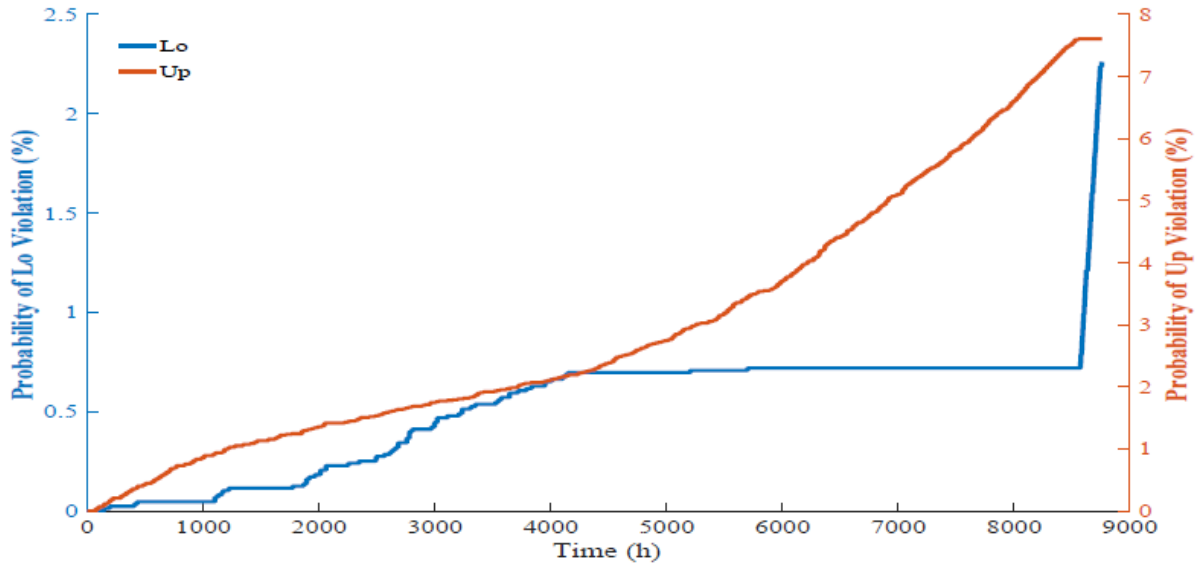

Fig. 24: Probability of violating upper and lower limits of BAT in 8760h with RLS+P PoPA

RLS+P PoPA ($y = Ax + B$)

Furthermore, RLS+P ($y = Ax + B$) which had the worst SLo violation of 1217 times, consequently also activated the DSL 673 times and the FC 2754 times. Thus, benchmarked against the performance of the DA PoPA utilising the RLS+P ($y = Ax + B$), led to 51.4% in SLo violation, 194% and 432% increase in DSL and FC activation as shown in Table 5 and in Figure 25. Thus, despite a decently sized HT of 15m3 (initialised with SOAccnHT at 80%), the SOAccnHT violated the 10% constraint limit on the HT; hence, causing the unavailability of the FC in periods requiring energy supply as shown in Figure 26. Nevertheless, the RLS+P ($y = Ax + B$) activated the PV 8582 times, which was a record high and also a 7.2% increase compared to the DA PoPA which activated the PV 8004 times as shown in Table 5. However, Figure 27 which shows the progression of the probability of violating the SLo and SUp insightfully reveals that the bulk of the SLo violation occurred after 5979 h as seen by the immediate steep rise in the SLo probability of violation from 4% to 14% due to lack of H2 carrier in the HT.

Therefore, investigating further with HT capacity of $25m^3$ confirms this assertion as the SLo violation reduces to 197 times which is a 75.5% decrease as shown in Table 5. Also, the SUp violation and DSL activation were decreased by 42.2% and 67.7% as well. Typical of a robust approach; the RLS+P (A=Ax+B) algorithm requires more allocation of H2 resources, which will consequently increase operational cost in contrast to the rest of the methods.

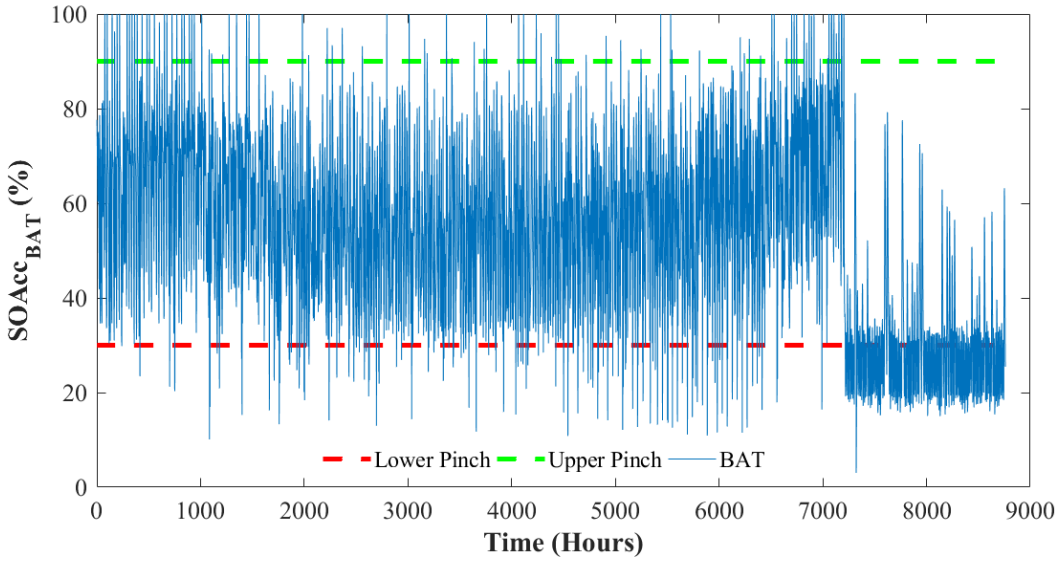

Fig. 25: 8760h BAT response with RLS+P PoPA with bias

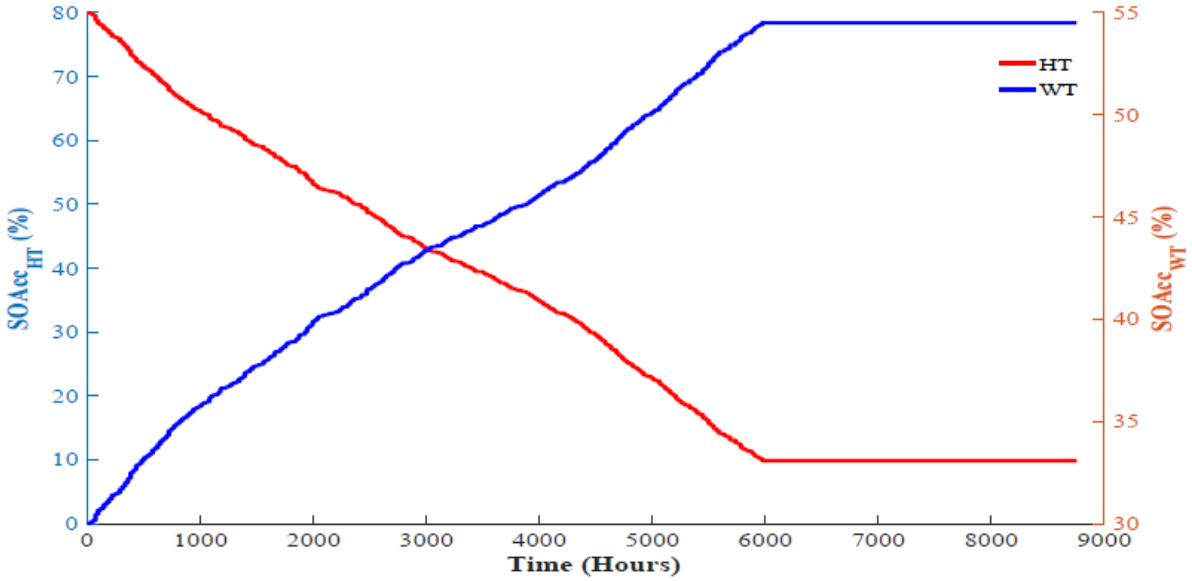

Fig. 26: HT and WT response for 8760h with RLS+P PoPA with bias

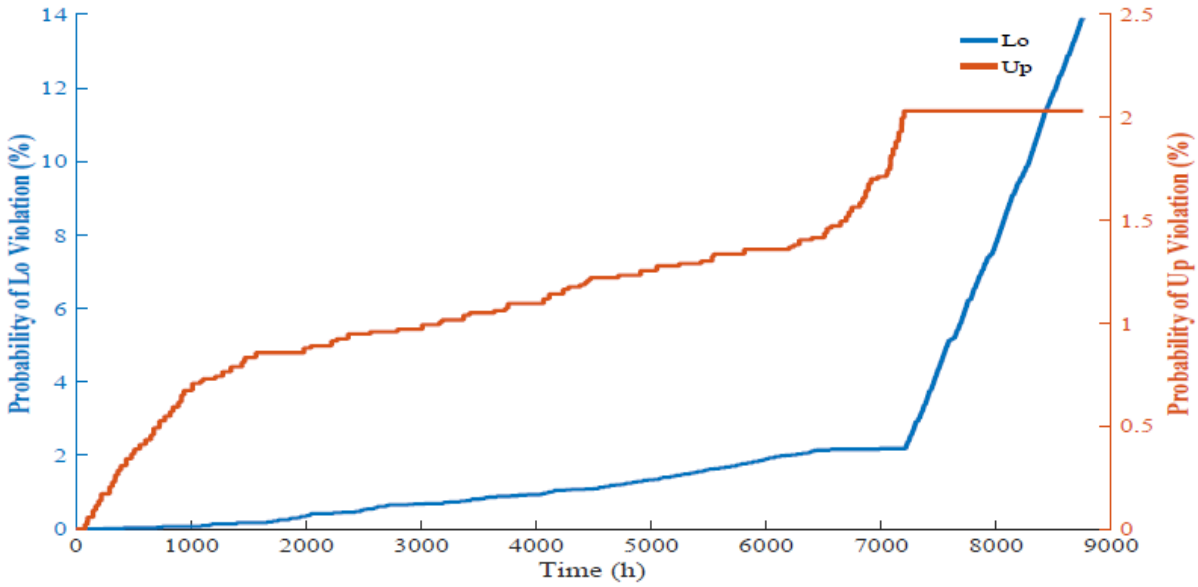

Fig. 27: Probability of violating upper and lower limits of BAT in 8760h with RLS+P PoPA with bias

Table 5: Summary of the EMS methods over 8760h under Non-Gaussian

Operational parameters	**PoPA EMS**						
	M1	**M2**	**M3**	**M4**	**M5**	**M6**	**M7**
Lower Pinch violation ($SOAcc_{BAT}^{n}$ < 30%)	804	271	64	51	321	198	1217
Upper Pinch violation ($SOAcc_{BAT}^{n}$>90%)	756	303	265	226	828	666	178
FC start-stop (cycles/year)	296	577	1837	3802	1935	2281	1574
EL start-stop (cycles/year)	262	654	931	3503	926	1253	1356
DSL start-stop (cycles/year)	229	1	0	0	126	79	673
PV start-stop (cycles/year)	8004	8457	8495	8534	7932	8094	8543

4.2.4 Long Term Analysis under Gaussian Uncertainty

P+Adaptive PoPA

The P+Adaptive PoPA had a better performance index of 202 times concerning the SLo compared to the DA and adaptive PoPA, which both had 876 and 209 violations. However, the P+Adaptive had the worst SUp violation of 813 times, which was a 5% increase compared to the DA PoPA's performance. Also, the DSL was activated 104 times, which was only marginally better than the DA PoPA's performance of 108 times, as shown in Table 6.

RLS+P PoPA ($y = Ax$)

The RLS-P PoPA with the simplest residual error linear model ($y = Ax$), had the second-best SLo performance of 15 times which was a tremendous improvement to the P+Adaptive PoPA which had 202 SLo violations as shown in Table 6. Also, compared with the performance of the DA to the RLS-P

PoPA ($y = Ax$), the SLo violation was reduced by 98%, and the SUp violation was also decreased by 22%. Furthermore, DSL was never activated; hence, a 100% reduction in fossil fuel emission was achieved with the RLS-PoPA. The FC and EL which were activated 1480 and 900 times was only utilised more compared to the DA and Adaptive PoPA EMS as shown in Table 6.

RLS-P PoPA ($y = Ax + B$)

The RLS-P PoPA with bias had the worse SLo performance, as shown in Table 6. Nonetheless, a further investigation which was carried out by increasing the HT capacity from 15m3 to 25m3 revealed the main reason for the sub-optimal performance of the RLS-P with a biased linear model was as a result of limited H2 resources. Therefore, with the HT at 25m3, the RLS-P PoPA with a first-order residual linear model, had an improved performance as the SLo violation and DSL activation 1023 reduced from 1023 to 235 times and from 510 to 86 times respectively. However, the SUp violation increased from 217 to 448 times. Nevertheless, the RLS-P PoPA with a first-order linear residual model as with a typical probabilistic approach introduces robustness which is only achieved at the cost of increased usage of H2 resources.

Table 6: Long Term Analysis under Gaussian Uncertainty

Operational parameters	**PoPA EMS**						
	M1	**M2**	**M3**	**M4**	**M5**	**M6**	**M7**
Lower Pinch violation ($SOAcc_{BAT}^{n}$ < 30%)	867	209	94	38	202	15	1023
Upper Pinch violation ($SOAcc_{BAT}^{n}$>90%)	777	287	229	216	813	609	217
FC start-stop (cycles/year)	264	550	1607	3087	2290	1480	2754
EL start-stop (cycles/year)	265	264	1113	3111	1149	900	1411
DSL start-stop (cycles/year)	108	0	0	0	104	0	510
PV start-stop (cycles/year)	7983	8473	8544	8490	7947	8151	8543

Tables 7 and 8 presents a quantitative summary of the percentage change between the performance of the DA-PoPA EMS reference, existing methods and the proposed methods under non-Gaussian and Gaussian uncertainty respectively. In Table 7 and 8, negative percentage change indicates a better performance and positive percentage increase signifies worsening performance excluding PV start-stop cycles where a decrease indicates a reduction in PV penetration or usage and vice versa.

Table 7: Percentage change in the performance of the proposed methods to the DA PoPA reference under non-Gaussian uncertainty and the HT sized at 15m3

Operational parameters	PoPA EMS					
	M2	**M3**	**M4**	**M5**	**M6**	**M7**
Lower Pinch violation ($SOAcc_{BAT}^{n}$ < 30%)	-66%	-92%	-94%	-60%	-75%	51%
Upper Pinch violation ($SOAcc_{BAT}^{n}$>90%)	-60%	-65%	-70%	10%	-12%	-76%
FC start-stop (cycles/year)	95%	521%	1184%	554%	671%	432%
EL start-stop (cycles/year)	150%	255%	1237%	253%	378%	418%
DSL start-stop (cycles/year)	-100%	-100%	-100%	-45%	-66%	130%
PV start-stop (cycles/year)	6%	6%	7%	-1%	1%	7%

Table 8: Percentage change in the performance of the proposed methods to the DA PoPA reference under Gaussian uncertainty and the HT sized at 15m3

Operational parameters	PoPA EMS					
	M2	**M3**	**M4**	**M5**	**M6**	**M7**
Lower Pinch violation ($SOAcc_{BAT}^{n}$ < 30%)	-76%	-89%	-96%	-77%	-98%	18%
Upper Pinch violation ($SOAcc_{BAT}^{n}$>90%)	-63%	-71%	-72%	5%	-22%	-72%
FC start-stop (cycles/year)	108%	509%	1069%	767%	461%	943%
EL start-stop (cycles/year)	174%	320%	1074%	334%	240%	432%
DSL start-stop (cycles/year)	-100%	-100%	-100%	-4%	-100%	372%
PV start-stop (cycles/year)	6%	7%	6%	0%	7%	7%

4.3 Analysis of Battery Degradation with PoPA EMS using Rainflow Counting Algorithm

The effect of uncertainty has been shown to potentially distort the shape of the PGCC which consequently results in the degradation of both full and/or partial life cycles in the BAT by fluctuating the depth of discharge (DoD) (i.e., the compliment of the state of charge of the BAT). Therefore, for accurate analysis of the BAT's life span or degradation both full and partial dis/charge cycles must also be considered.

Hence, the rainflow-counting algorithm for analysing fatigue/stress analysis in materials [71], has been adapted to count the number of cycles (both full and partial) with respect to the depth of discharge pattern which were determined by the EMS algorithms. The rainflow-counting algorithm considers both full and partial counts with respect to the state of charge of the battery which can be interpreted as a compliment of the depth of discharge.

Experimental data for life cycle versus different depths of discharge rates obtained in [72] was used to determine a regression model, $f(DoD)$ with norm of residuals validated as $3.4127e-11$ via cubic curve fitting in this work.

Total number of cycles, $f(DoD) = p1 * DoD^3 + p2 * DoD^2 + p3 * DoD + p4$ (32)

Where, the coefficients of the cubic polynomial regression model are; $p1 = -0.09375$, $p2 = 22.396$, $p3 = -1868.8$, $p4 = 59167$.

Figure 28, shows the model versus the empirical data for DoD relationship with respect to lithium Battery life cycles

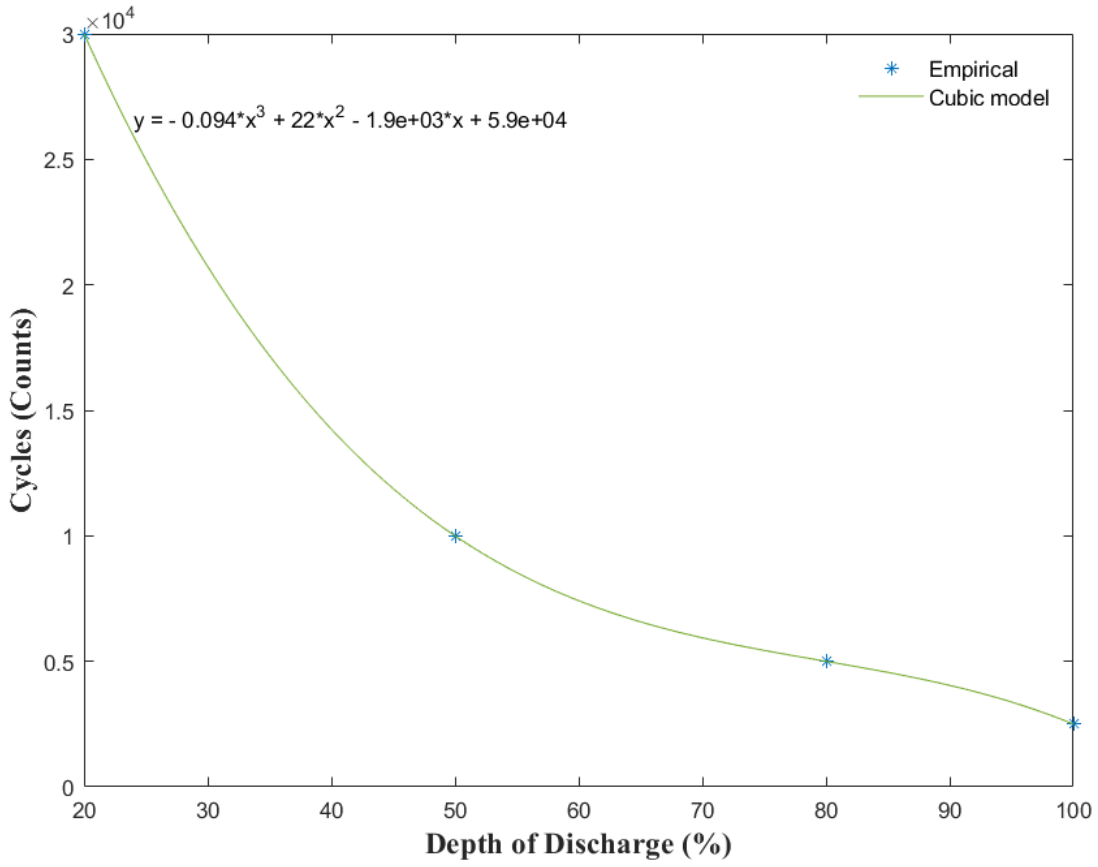

Fig 28: Battery Life Cycle with respect to Depth of Discharge [72]

The remaining battery life cycle at time k is modelled as the difference between the initial battery life cycle at time $k-1$, and the total degraded life cycle during the operation of the battery. The total degraded life cycle during the operation of the battery is the cumulative sum obtained from the normalised reciprocal of life cycle with respect to DoD multiplied by the equivalent rainflow DoD cycle count. It is important to note that cycles incurred with larger DoD in contrast to a small DoD, will have more detrimental impact on the BAT lifespan. The remaining battery cycle lifespan is expressed mathematically as follows:

$$T_{cyc}^{R}(k) = T_{cyc}^{R}(k-1) - \sum_{q=1}^{Q}\left(\left[T_{cyc}^{max} \Big/ f\left(DoD(q)\right)\right] * \delta(DoD(q))\right) \quad (33)$$

Where, the number of DoD bins with an incurred cycle count is $q \in [1 - Q]$ computed in Appendix Table A4 and A5, $\delta(DoD)$ is the number of cycles function obtained using rainflow-counting algorithm with respect to the depth of discharge range (bin width). While, $f(DoD)$ computed in Appendix Table A6, is the cubic regression model function of the lithium-ion battery's maximum life cycle with respect to DoD. However, for consistency with the cycle counts obtained as per histogram bin width resolution using rainflow counting algorithm, the average DoD or the centre of bin width is used with $f(DoD)$. And T_{cyc}^{max} is the total life cycle count in the battery at initialisation which is obtained as 5.9e-04 by evaluating $f(DoD)$ with DoD at 0%.

The remaining BAT capacity is expressed as the difference between the initial BAT capacity and the ratio of degraded BAT cycles and the total BAT cycles at initialisation scaled by the nominal BAT capacity as follows:

$$\text{Remaining Battery Capacity } (Wh) = C_{BAT}\left(1 - \left[{T_{cyc}^{R}}/{T_{cyc}^{max}}\right]\right) \quad (34)$$

While, the percentage of the battery's degraded capacity is expressed as follows:

$$\text{Degraded Battery Capacity (\%)} = \text{Degraded Battery Capacity } (Wh) * 100/C_{BAT} \quad (35)$$

The degradation of the BAT over 8760h with respect to life cycles depletion and its equivalent percentage decrease in the overall battery capacity is presented in Table 9. The benchmark DA-PoPA (M1) has the least degradation with respect to cycles lost during the yearly operation under both non-/Gaussian uncertainty by 4.3% and 4.13% respectively. Nevertheless, the RLS (y=Ax) which was had 5.43% degradation, depleted only 677 cycles more than the DA-PoPA with an overall better performance under gaussian uncertainty and similarly only 5.5% of the total cycle count was degraded under non-Gaussian uncertainty. Furthermore, the P+Adaptive (M5) and RL (M4) PoPA degraded the battery the most under non-Gaussian and Gaussian uncertainty by 6.74% and 6.47% respectively.

Table 9: Yearly (8760 h) Battery Capacity Degradation with PoPA - EMS algorithms

Battery lifetime index	**M1**	**M2**	**M3**	**M4**	**M5**	**M6**	**M7**
Remaining Battery Life cycle under Gaussian uncertainty (counts)	57037	56231	56944	55746	55939	56362	56075
Degraded Battery Capacity under Gaussian Uncertainty (%)	4.30	5.65	4.46	6.47	6.14	5.43	5.91
Remaining Battery Life cycle under non-Gaussian uncertainty (counts)	57,139	56,359	56,193	55,983	55,584	56,320	56,190
Degraded Battery Capacity under Non-Gaussian Uncertainty (%)	4.13	5.44	5.72	6.07	6.74	5.50	5.72

5. Conclusions

Three Probabilistic+Adaptive PoPA strategies were proposed for energy management of HESS uncertainty which uses a stochastic process based on Monte Carlo simulation. The Monte Carlo simulation was enabled by historical data and decent computer processing speed (intel Core i5). Analysis with Gaussian uncertainty showed the proposed RLS+P (y=Ax) method performed better in clipping the PGCC from violating the SLo (i.e. over-discharging the BAT below 30%) in contrast to the reference DA, Adaptive and Kalman +Adaptive PoPA, state of the art RL+Adaptive PoPA methods which utilised the average PV and load data for prediction. Nevertheless, the RL+adaptive PoPA method which had the best performance with over-charging the BAT beyond 90%, was only negligibly better than the RLS+P (y=Ax+B) method.

However, under non-Gaussian uncertainty, the utilisation of hydrogen increased with the proposed methods which resulted in increased violation of the lower operating limit of the BAT due to hydrogen unavailability which consequently led to frequent DSL activation. This is not unexpected since Monte Carlo simulation assumes the uncertainty is of Gaussian distribution. Nevertheless, the RLS+P with bias showed better performance with preventing over-charging of the BAT, the RL+Adaptive PoPA EMS has better performance with lower BAT limit violation and no DSL usage under non-Gaussian uncertainty.

The DA had the least battery degradation of 4.3% and 4.13% which was better than the RLS+P (y=Ax) by 1.1% and 1.4% under both Gaussian and non-Gaussian uncertainty respectively. Regardless of the DA having the least degradation indices, the DA-PoPA activated the DSL the most due to the frequent cycling of the battery at small DoD within the lower operating limit.

Therefore, the probabilistic Adaptive EMS RLS+P ($y = Ax$) which uses MCS with historical data rather than average PV and load demand profiles like in existing PoPA EMS can conservatively enhance reliability in off-grid HESS particularly under Gaussian uncertainty. Also, the proposed methods, satisfied the operational constraints which enforces conservation of the hydrogen resources, while limiting both the impact of battery degradation and carbon emission from the DSL.

Acknowledgement

B.E Nyong-Bassey would like to thank Petroleum Development Technology Funds, Nigeria (PTDF/ED/OSS/PHD/SLA/818/16) for their support towards this work. Dr. Damian Giaouris would like to acknowledge the support from the EPSRC National Centre for Energy Systems Integration (CESI) (Grant No.: EP/P01173/1).

References

[1] M. S. Adaramola, S. S. Paul, and O. M. Oyewola, "Assessment of decentralized hybrid pv solar-diesel power system for applications in northern part of nigeria," Energy for Sustainable Development, vol. 19, pp. 72–82, 2014.

[2] A. Q. Jakhrani, A. K. Othman, A. R. H. Rigit, S. R. Samo, and S. A. Kamboh, "A novel analytical model for optimal sizing of standalone photovoltaic systems," Energy, vol. 46, no. 1, pp. 675–682, 2012.

[3] P. Nema, R. Nema, and S. Rangnekar, "A current and future state of art development of hybrid energy system using wind and pv-solar: A review," Renewable and Sustainable Energy Reviews, vol. 13, no. 8, pp. 2096–2103, 2009.

[4] K. Ajao, O. Oladosu, and O. Popoola, "Using homer power optimization softwarefor cost benefit analysis of hybrid-solar power generation relative to utility cost in nigeria," International Journal of Research and Reviews in Applied Sciences, vol. 7, no. 1, p. 14, 2011.

[5] S. Hajiaghasi, A. Salemnia, and M. Hamzeh, "Hybrid energy storage system for microgrids applications: A review," Journal of Energy Storage, vol. 21, pp. 543–570, 2019.

[6] T. Bocklisch, "Hybrid energy storage systems for renewable energy applications," Energy Procedia, vol. 73, pp. 103–111, 2015.

[7] D. Giaouris, A. I. Papadopoulos, C. Ziogou, D. Ipsakis, S. Voutetakis, S.Papadopoulou, P. Seferlis, F. Stergiopoulos, and C. Elmasides, "Performance investigation of a hybrid renewable power generation and storage system using systemic power management models," Energy, vol. 61, pp. 621–635, 2013.

[8] X. Feng, H. Gooi, and S. Chen, "Hybrid energy storage with multimode fuzzy power allocator for pv systems," IEEE Transactions on Sustainable Energy, vol. 5, no. 2, pp. 389–397, 2014.

[9] L. W. Chong, Y. W. Wong, R. K. Rajkumar, and D. Isa, "An optimal control strategy for standalone pv system with battery-supercapacitor hybrid energy storage system,"Journal of Power Sources, vol. 331, pp. 553–565, 2016.

[10] A. Maleki and F. Pourfayaz, "Sizing of stand-alone photovoltaic/wind/diesel system with battery and fuel cell storage devices by harmony search algorithm," Journal of Energy Storage, vol. 2, pp. 30–42, 2015.

[11] V. Dash and P. Bajpai, "Power management control strategy for a stand-alone solar photovoltaic-fuel cell–battery hybrid system," Sustainable Energy Technologies and Assessments, vol. 9, pp. 68–80, 2015.

[12] S. Nasri, B. S. Sami, and A. Cherif, "Power management strategy for hybrid autonomous power system using hydrogen storage," International Journal of Hydrogen Energy, vol. 41, no. 2, pp. 857–865, 2016.

[13] T. Alnejaili, S. Drid, D. Mehdi, L. Chrifi-Alaoui, R. Belarbi, and A. Hamdouni, "Dynamic control and advanced load management of a stand-alone hybrid renewable power system for remote housing," Energy Conversion and Management, vol. 105, pp. 377–392, 2015.

[14] S. Sikkabut, P. Mungporn, C. Ekkaravarodome, N. Bizon, P. Tricoli, B. Nahid-Mobarakeh, S. Pierfederici, B. Davat, and P. Thounthong, "Control of high-energy high-power densities storage devices by li-ion battery and supercapacitor for fuel cell/photovoltaic hybrid power plant for autonomous system applications," IEEE Transactions on Industry Applications, vol. 52, no. 5, pp. 4395–4407, 2016.

[15] D. Ipsakis, S. Voutetakis, P. Seferlis, F. Stergiopoulos, and C. Elmasides, "Power management strategies for a stand-alone power system using renewable energy sources and hydrogen storage," International journal of hydrogen energy, vol. 34, no. 16, pp. 7081–7095, 2009.

[16] J. Bernard, S. Delprat, F. Buechi, and T. M. Guerra, “Global optimisation in the power management of a fuel cell hybrid vehicle (fchv),” in 2006 IEEE Vehicle Power and Propulsion Conference, pp. 1–6, IEEE, 2006.

[17] E. Eriksson and E. M. Gray, “Optimization and integration of hybrid renewable energy hydrogen fuel cell energy systems–a critical review,” Applied energy, vol. 202, pp. 348–364, 2017.

[18] S. Arens, S. Schlüters, B. Hanke, K. Von Maydell, and C. Agert, ‘‘Monte-Carlo Evaluation of Residential Energy System Morphologies Applying Device Agnostic Energy Management’’, *IEEE Access*, *10*, 7460-7475, 2021.

[19] F. Tooryan, H. HassanzadehFard, E.R. Collins, S. Jin, and B. Ramezani0 ‘‘Optimization and energy management of distributed energy resources for a hybrid residential microgrid’’ Journal of Energy Storage, 30, p.101556, 2020.

[20] Y. Shen, Y. Li, Y. Tang, J. Sun, J. Zhao, J. and X. Yang, ‘‘An energy management strategy based on fuzzy logic for hybrid energy storage system in electric vehicles. *IEEJ Transactions on Electrical and Electronic Engineering*, *17*(1), 53-60, 2022.

[21] A. Aktas, K. Erhan, S. Özdemir, E. Özdemir, ‘‘Dynamic energy management for photovoltaic power system including hybrid energy storage in smart grid applications’’, Energy, vol. 162, p72-82. 2018.

[23] Z. Luo, W. Gu, Z. Wu, Z. Wang, Y. Tang, ‘‘A robust optimization method for energy management of CCHP microgrid. Journal of Modern Power Systems and Clean Energy, vol. 6(1), p132-144. 2018.

[24] Y. Zhang, L. Fu, W. Zhu, X. Bao, C. Liu, ‘‘Robust model predictive control for optimal energy management of island microgrids with uncertainties’’, Energy, vol. 164, p1229-1241, 2018.

[25] M. A. Hossain, H. R. Pota, S. Squartini, and A. F. Abdou, ‘‘Modified PSO algorithm for real-time energy management in grid-connected microgrids,’’ Renew. Energy, vol. 136, pp. 746–757, Jun. 2019.

[26] Y. Du and F. Li, ‘‘Intelligent multi-microgrid energy management based on deep neural network and model-free reinforcement learning,’’ IEEE Trans. Smart Grid, vol. 11, no. 2, pp. 1066–1076, Mar. 2020.

[27] B.E. Nyong-Bassey, D. Giaouris, C. Patsios, S. Papadopoulou, A.I. Papadopoulos, S. Walker, S. Voutetakis, P. Seferlis, S. Gadoue, ‘‘Reinforcement learning based adaptive power pinch analysis for

energy management of stand-alone hybrid energy storage systems considering uncertainty'', Energy. Vol.193, p116622, 2020

[28] O. Gomozov, J. P. F. Trovão, X. Kestelyn and M. R. Dubois, "Adaptive Energy Management System Based on a Real-Time Model Predictive Control With Nonuniform Sampling Time for Multiple Energy Storage Electric Vehicle," in *IEEE Transactions on Vehicular Technology*, vol. 66, no. 7, pp. 5520-5530, 2017.

[29] H. Chen, R. Xiong, C. Lin, and W. Shen ''Model predictive control based real-time energy management for hybrid energy storage system'', *CSEE Journal of Power and Energy Systems*, *7*(4), 862-874, 2020.

[30] W. Hu, Q. Shang, X. Bian, and R. Zhu, ''Energy management strategy of hybrid energy storage system based on fuzzy control for ships'', *International Journal of Low-Carbon Technologies*, *17*, pp.169-175, 2022.

[31] Y. Shen, Y. Li, Y. Tang, J. Sun, J. Zhao, and X. Yang, X, ''An energy management strategy based on fuzzy logic for hybrid energy storage system in electric vehicles'', *IEEJ Transactions on Electrical and Electronic Engineering*, *17*(1), pp.53-60, 2022.

[32] J. M. Buhmann, A. Y Gronskiy, M. Mihalák, T. Pröger, R. Šrámek, P. Widmayer, ''Robust optimization in the presence of uncertainty: A generic approach'', Journal of Computer and System Sciences, vol. 94, p135-166, 2018.

[33] J. He, C. Shi, T. Wei, X. Peng, Y. Guan, ''Hierarchical optimal energy management strategy of hybrid energy storage considering uncertainty for a 100% clean energy town'', *Journal of Energy Storage*, *41*, 102917, 2021

[34] V. S. Tabar, M. A. Jirdehi, R. Hemmati, ''Energy management in microgrid based on the multi objective stochastic programming incorporating portable renewable energy resource as demand response option'', Energy, vol. 118, p827-839, 2017.

[35] M.C. Hu, S.Y. Lu, Y.H. Chen, ''Stochastic programming and market equilibrium analysis of microgrids energy management systems'', Energy, vol. 113, p662-670. 2016;

[36] A. Lahyani, R. Abdelhedi, A. C. Ammari, A. Sari, P. Venet, ''Reinforcement learning based adaptive power sharing of battery/supercapacitors hybrid storage in electric vehicles'', *Energy Sources, Part A: Recovery, Utilization, and Environmental Effects*, 1-22, 2020.

[37] J. Duan, Z. Yi, D. Shi, C. Lin, X. Lu, and Z. Wang, ''Reinforcement-learning-based optimal control of hybrid energy storage systems in hybrid AC–DC microgrids'',*IEEE Transactions on Industrial Informatics*, *15*(9), 5355-5364, 2019

[38] D. Giaouris, A. I. Papadopoulos, P. Seferlis, S. Voutetakis, and S. Papadopoulou, “Power grand composite curves shaping for adaptive energy management of hybrid microgrids,” Renewable energy, vol. 95, pp. 433–448, 2016.

[39] B.E. Nyong-Bassey, D. Giaouris, A. I. Papadopoulos, H. Patsios, S. Papadopoulou, S. Voutetakis, P. Seferlis, S. Walker, P. Taylor, and S. Gadoue, “Adaptive power pinch analysis for energy management of hybrid energy storage systems,” in 2018 IEEE International Symposium on Circuits and Systems (ISCAS), pp. 1–5, IEEE, 2018.

[40] B. Linnhoff, and J.R. Flower, ‘‘Synthesis of heat exchanger networks: I. Systematic generation of energy optimal networks’’, *AIChE Journal, 24*(4), 633-642, 1978.

[41] N. M. Rozali, Z. A. Manan, S. W. Alwi, and J. J. Klemeš, ‘‘Supply Planning and Demand Management of Hybrid Power Systems Using Process Integration’’, pp. 167-178, 2017.

[42] A. Chawla, F. Bühler, and B. Elmegaard, ‘‘A practical approach to performing Pinch Analysis followed by Heat Exchanger Network retrofit of an oil refinery’’, In *5th International Conference on Smart Energy Systems in Copenhagen*, 2019.

[43] L. Čuček, S. Boldyryev, J.J. Klemeš, Z. Kravanja, G. Krajačić, P.S. Varbanov, and N. Duić, ‘‘Approaches for retrofitting heat exchanger networks within processes and Total Sites’’, *Journal of Cleaner Production, 211*, 884-894, 2019.

[44] H. H. Chin, P. Y. Liew, P. S. Varbanov, and J. J. Klemeš, ‘‘Extension of pinch analysis to targeting and synthesis of water recycling networks with multiple contaminants’’, *Chemical Engineering Science, 248*, 117223, 2022.

[45] N. M. Farrag, D. A. Kamel, A. O. Ghallab, M. A. Gadalla, and M. K. Fouad, M. K., ‘‘Graphical Design and Analysis of Mass Exchange Networks Using Composition Driving Forces’’, *South African Journal of Chemical Engineering, 36*, 94-104, 2021.

[46] G. Shukla, and N.D Chaturvedi, ‘‘A Pinch Analysis approach for minimizing compression energy and capital investment in gas allocation network’’, *Clean Technologies and Environmental Policy, 23*(2), 639-652, 2021.

[47] S. Bandyopadhyay, N. D. Chaturvedi, A. Desai, ‘‘Targeting compression work for hydrogen allocation networks’’, *Industrial & Engineering Chemistry Research, 53*(48), 18539-18548, 2014.

[48] N. D. Chaturvedi, ‘‘Cost-optimal pinch analysis for sizing of hybrid power systems’’, *Cleaner Engineering and Technology, 3*, 100094, 2021.

[49] N. E. M. Rozali, S. R. W. Alwi, Z. A. Manan, J. J. Klemeš, and M. Y. Hassan, ‘‘Process Integration techniques for optimal design of hybrid power systems’’, *Applied Thermal Engineering, 61*(1), 26-35, 2013.

[50] S. Bandyopadhyay, “Design and optimization of isolated energy systems through pinch analysis,” Asia-Pacific Journal of Chemical Engineering, vol. 6, no. 3, pp. 518–526, 2011.

[51] S. Norbu and S. Bandyopadhyay, “Power pinch analysis for optimal sizing of renewable-based isolated system with uncertainties,” Energy, vol. 135, pp. 466–475, 2017.

[52] Y. Zhang, Z. Yan, C. C. Zhou, T. Z. Wu, and Y. Y. Wang, Y. Y. ‘‘Capacity allocation of HESS in micro-grid based on ABC algorithm. *International Journal of Low-Carbon Technologies’’, 15*(4), 496-505, 2020.

[53] G. Mavrotas, K. Florios, and D. Vlachou, “Energy planning of a hospital using mathematical programming and monte carlo simulation for dealing with uncertainty in the economic parameters,” Energy Conversion and Management, vol. 51, no. 4, pp. 722–731, 2010.

[54] W. Du, “Model validation by statistical methods on a monte-carlo simulation of residential low voltage grid,” in Future Communication, Computing, Control and Management, pp. 93–98, Springer, 2012.

[55] E. J. da Silva Pereira, J. T. Pinho, M. A. B. Galhardo, and W. N. Macedo, “Methodology of risk analysis by monte carlo method applied to power generation with renewable energy,” Renewable Energy, vol. 69, pp. 347–355, 2014.

[56] B.E. Nyong-Bassey, D. Giaouris, H. Patsios, S. Gadoue, A. I. Papadopoulos, P. Seferlis, S. Voutetakis, and S. Papadopoulou, “Probabilistic adaptive model predictive power pinch analysis (popa) energy management approach to uncertainty,” The Journal of Engineering, 2019.

[57] B. R. Prusty and D. Jena, “A critical review on probabilistic load flow studies in uncertainty constrained power systems with photovoltaic generation and a new approach,” Renewable and Sustainable Energy Reviews, vol. 69, pp. 1286–1302, 2017.

[58] Chalmers university of technology, TMS150/MSG400, ‘‘stochastic data processing and simulation 2018.” http://www.math.chalmers.se/Stat/Grundutb/CTH/tms150/1516/MC_ 20151008.pdf. [Online; accessed 19-July-2019].

[59] P. gremaud, ‘‘Advanced numerics and modeling in science and engineering’’, north carolina state university, http://www4.ncsu.edu/~gremaud/ MA798C/mc.pdf. [Online; accessed 10-July-2018].

[60] A. Gramacki, ‘‘Nonparametric kernel density estimation and its computational aspects’’, Cham: Springer International Publishing; 2018.

[61] J. S. Galpin and D. M. Hawkins, “The use of recursive residuals in checking model fit in linear regression,” The American Statistician, vol. 38, no. 2, pp. 94–105, 1984.

[62] F. Kianifard and W. H. Swallow, “A review of the development and application of recursive residuals in linear models,” Journal of the American Statistical Association, vol. 91, no. 433, pp. 391–400, 1996.

[63] “ELEXON.” http://data.ukedc.rl.ac.uk/simplebrowse/edc/efficiency/residential/ LoadProfile/data. [Online; accessed 19-July-2019].

[64] “NREL.” http://pvwatts.nrel.gov/pvwatts.php. [Online; accessed 19-July-2019].

[65] G. Mavrotas, K. Florios, and D. Vlachou, “Energy planning of a hospital using mathematical programming and monte carlo simulation for dealing with uncertainty in the economic parameters,” Energy Conversion and Management, vol. 51, no. 4, pp. 722–731, 2010.

[66] P. Pflaum, M. Alamir, and M. Y. Lamoudi, “Probabilistic energy management strategy for ev charging stations using randomized algorithms,” IEEE Transactions on Control Systems Technology, vol. 26, no. 3, pp. 1099–1106, 2017.

[67] V. A. Epanechnikov, “Non-parametric estimation of a multivariate probability density,” Theory of Probability & Its Applications, vol. 14, no. 1, pp. 153–158, 1969.

[68] M. Y. Ata, “Determining the optimal sample size in the Monte Carlo experiments,” Selcuk Journal of Applied Mathematics, vol. 7, no. 2, pp. 103–111, 2006.

[69] W. Du, “Model validation by statistical methods on a Monte-Carlo simulation of residential low voltage grid,” in Future Communication, Computing, Control and Management, pp. 93–98, Springer, 2012.

[70] D. Ding, A. Gandy, and G. Hahn, “A simple method for implementing Monte Carlo tests,” arXiv preprint arXiv:1611.01675, 2016.

[71] ASTM E1049-85 (2017), “Standard practices for cycle counting in fatigue analysis”, West Conshohocken, PA: ASTM International, 2011 [online; accessed 4th of May 2022 https://www.astm.org/cgi-bin/resolver.cgi?E1049].

[72] K. R. Mallon, F. Assadian, and B. Fu, ‘‘Analysis of on-board photovoltaics for a battery electric bus and their impact on battery lifespan. *Energies*, *10*(7), 943, 2017.